MINISTERIO DE MINAS Y ENERGIA

ESTUDIO DE LA PROPAGACION DE LA ONDA ONDA DE PRESION

2006

553

Estudio de la Propagación de la Onda de Presión y del Proceso de Despresurización para un Transformador Eléctrico Sometido a un Arco Interno

Diseño de una Herramienta de Gestión para la Toma de Decisiones para la Prevención de Explosión de Transformadores

Guillaume PERIGAUD (Director del Departamento de Investigaciones)
Héloïse CUNY (Ingeniera del Departamento de Investigaciones)
Sylvain PRIGENT (Director del Departamento de Desarrollo)
Philippe MAGNIER (Presidente)
SERGI Holding, 186 av. Du Général de Gaulle, 78260 ACHERES, FRANCIA

Resumen

Los transformadores eléctricos de aceite pueden ser sometidos a fallas de baja impedancia, lo que conlleva por lo general a la ruptura del tanque del transformador. SERGI diseñó y vende el TRANSFORMER PROTECTOR (TP) que evita dichos eventos dramáticos. Para probar la eficacia del TP en el 2002 Electricité de France (EDF) realizó en su laboratorio de alto voltaje la primera campaña de pruebas para arcos en transformadores pequeños. La segunda campaña fue llevada a cabo en el 2004 por CEPEL, laboratorio de alto voltaje brasileño, en tres transformadores de talla industrial, cada uno equipado con un TP. Durante las dos campañas, se realizaron sesenta y dos pruebas, todas con éxito; el TP despresurizó el tanque del transformador evitando la explosión en cada prueba. Las pruebas demostraron de manera experimental, la eficacia y la confiabilidad del TP. Sin embargo, dado que cada configuración física no puede ser probada, SERGI ha desarrollado desde 1995 una herramienta de simulación, el Modelo MTH (Magneto-Termo-Hidrodinámico) que demostró de manera numérica la confiabilidad del TP para numerosas situaciones críticas. Este modelo ha sido actualizado para tomar en cuenta fenómenos muy transitorios como las ondas de presión, su propagación en el aceite del transformador y su interacción con la estructura del tanque. En este artículo que describe esta modelación actualizada, el aceite y el gas son considerados como medios compresibles. Un modelo euleriano para un fluido difásico compresible es así detallado en este artículo así como también las hipótesis de modelación física. Las características termodinámicas de cada material son expuestas. Diversos efectos físicos como la gravedad, viscosidad, transferencias de calor e influencias de los arcos en presiones locales son igualmente modeladas. Una herramienta numérica en dos dimensiones es presentada: la geometría está dividida en pequeños dominios de cálculos individualizados por una malla estructurada lo que permite explicar la geometría compleja del transformador. Los métodos numéricos dedicados a calcular las contribuciones de los diferentes efectos son también tratados: los "solvers" de Riemann, los esquemas numéricos de los efectos viscosos, térmicos y de gravedad son detallados. Se procura una atención particular al tratamiento numérico de las condiciones de los límites, y especialmente a la descripción y a la influencia numérica del TP: condiciones de límites específicas son compuestas para describir de manera precisa el TP. Las ventajas de tal método son aplicadas. Las capacidades de la herramienta numérica son ilustradas mediante una comparación cualitativa entre las evoluciones temporales de presión experimental y simulada relativas a las pruebas de creación de arco efectuadas en EDF. Las presiones modeladas y experimentales están en acuerdo cualitativo: las fases de evolución temporal de presión exhibidas por las experiencias son predichas por la herramienta de simulación en función de la energía transferida por el arco al aceite. El estudio cuantitativo completo y la validación de la herramienta no son presentadas en este documento pero son el objeto de otro artículo [21]. El modelo y el método numérico son capaces para representar de manera precisa la propagación de onda de presión y la influencia del TP es probada mediante las simulaciones.

PREVENCION CONTRA LA EXPLOSION E INCENDIO DE TRANSFORMADORES
Pruebas en Vivo en Transformadores Grandes: Análisis y Simulaciones

Guillaume PERIGAUD (Director del Departamento de Investigaciones)
Héloïse CUNY (Ingeniera del Departamento de Investigaciones)
Sylvain PRIGENT (Director del Departamento de Desarrollo)
Philippe MAGNIER (Presidente)

SERGI Holding, 186 av. Du Général de Gaulle, 78260 ACHERES, Francia
E-mail: research@sergi-france.com, Web site: www.sergi-france.com

Resumen

Un paso fundamental para SERGI es mostrar le eficacia del TRANSFORMER PROTECTOR (TP) para todo transformador y todo tipo de ruptura de aislamiento. Es por eso que la filosofía del programa de investigación consiste en mantener una fuerte conexión entre las experiencias y los desarrollos teóricos.

Hasta hoy, se han realizado dos campañas de pruebas del TP, ambas bajo las peores condiciones mediante la creación de fallas de baja impedancia conllevando a arcos eléctricos dentro del aceite dieléctrico del tanque del transformador. En 2002, Electricité de France efectuó 28 pruebas al TP. Luego en el 2004, se efectuó una segunda campaña de 34 pruebas al TP. Estas fueron llevadas a cabo por CEPEL, el Laboratorio de Alto Voltaje en Brasil. Para las 62 pruebas, cada transformador estuvo equipado con el TP, que reacciona directamente a la propagación del pico de presión dinámico, onda de choque ocasionada por una falla de baja impedancia.

Durante las dos campañas de pruebas del TP, los fenómenos descritos con el Modelo Magneto-Termo-Hidrodinámico (MTH) de SERGI fueron confirmados y los resultados son presentados en este artículo.

El volumen de gas generado durante un arco eléctrico es una función logarítmica de la energía del arco. La producción del gas es muy elevada cuando el arco eléctrico se crea debido al intercambio intenso de calor entre el arco y el aceite dieléctrico. Tan pronto como se produce el gas, el arco es parcial o completamente rodeado de gas. Como resultado, la energía del arco es utilizada para calentar el gas, fragmentar el vapor de aceite en moléculas más pequeñas y transformar esos gases generados en plasma. Así, menos energía se transfiere al aceite para lograr su evaporación. En consecuencia, el primer Mega Joule transmitido al aceite dieléctrico genera *2.3 m3 (81.2''t3)* de gas explosivo, mientras que por un arco eléctrico de 100 MJ los otros 99 MJ contribuyen a la generación de solamente *2.0 m3 (71.1''t3).*

La aceleración más alta del tanque del transformador es alcanzada cuando se crea el arco eléctrico, cuando líquido es repentina e intensamente vaporizado. Durante estas pruebas, se observo que para un transformador de 72 toneladas de peso la aceleración alcanzó más de *400 g (g=9.81 m/s² i.e. 32.2 ft/s²),* demostrando que las fallas aplicadas son bastante considerables.

Cuando ocurre un arco eléctrico, sólo se genera un pico de presión. La transferencia de energía inicial es casi instantánea, así como también lo es el cambio de fase, de líquido a gas. Debido a la inercia del aceite, el gas es rápidamente presurizado. Dado que es más difícil vaporizar un líquido que fragmentar el vapor de aceite en moléculas más pequeñas, el arco eléctrico permanecería localizado principalmente en la fase gaseosa y se generará menos gas. Como consecuencia, cuando se comparan las pruebas para las cuales los picos de presión equivalen respectivamente a *8 bar (116 psi)* y *8.8 bar (127 psi),* las energías del arco correspondientes varían en un orden de magnitud de 10 (*0.1 MJ* y *1 MJ* respectivamente).

La correlación de los resultados obtenidos entre la energía del arco y la presión dinámica demuestra que la energía del arco no es el parámetro clave durante la explosión del tanque del transformador lo cual se opone a las creencias habituales de los ingenieros eléctricos.

Uno de los objetivos de las pruebas de CEPEL fue demostrar que el tanque resiste la onda de presión dinámica antes que el TP despresurice el tanque. La resistencia del tanque a la presión dinámica fue así experimentada para picos de presión hasta 10 veces superiores al límite de presión estática y durante 4 veces más largas que en el interior del transformador existente más grande. Para llegar a este resultado, se incorporó aire al aceite dado que 1% de aire en el aceite dieléctrico reduce la velocidad de la onda de choque por un factor 10, de 1200m/s a 128m/s. Durante las pruebas, el tiempo de activación más alto del TP fue 57 milisegundos para una onda de choque que se propagó a una distancia de 4 metros (m). Con aceite normal, es decir no contaminado, el tiempo de activación del TP sería de 6 milisegundos. En este caso, el tanque ha resistido la presión dinámica 10 veces más en tiempo que en aceite no contaminado. A modo de ejemplo, con aceite normal, 57 milisegundos corresponden a una distancia de propagación de la onda de choque de *68 m (220'')*. Un transformador que permita tal distancia no existe ya que debería ser 4.5 veces más grande que el transformador de *750MVA* utilizado aquí para las simulaciones.

La habilidad del TRANSFORMER PROTECTOR para evitar la explosión del tanque durante fallas de baja impedancia ha sido demostrada. Gracias a la baja inercia del TP para operar comparada al tiempo para la ruptura del tanque, la sobre presión en el tanque del transformador regresa al nivel de calibración de la presión estática en 3 milisegundos luego de la activación del TP. Esto confirma el valor obtenido de 3.5 milisegundos con el Modelo MTH y publicado por SERGI en el 2001.

Durante las 62 pruebas, el TP siempre evitó la explosión del transformador y todo tipo de daños o deformaciones permanentes en el tanque.

Otro de los objetivos importantes de CEPEL fue de comparar los resultados experimentales a las simulaciones efectuadas gracias a un programa exhaustivo que considera la propagación de la onda de presión y la influencia del TP. Para estas simulaciones, se adaptó un modelo de fluido bifásico compresible para actualizar el Modelo MTH de SERGI.

Se consideraron diferentes efectos físicos (compresibilidad, viscosidad, gravedad, influencia del arco y transferencia de calor). Pruebas numéricas respecto al transformador más grande utilizado para las pruebas de CEPEL son mostradas para realizar una comparación con las experimentaciones. La fuerte interacción entre la teoría y las experimentaciones conducen a la validación de la herramienta numérica así como del modelo físico y de las reglas empíricas. La utilización simultánea de simulaciones numéricas y de datos experimentales permiten esclarecer numerosos resultados en lo que respecta el volumen de gas generado por un arco eléctrico, la influencia de la geometría, la propagación de la onda de presión y de los picos de presión.

La despresurización de tanques de transformadores grandes es estudiada numéricamente cuando se consideran condiciones de fallas eléctricas extrapoladas. Para la propagación de la onda de choque, el peor caso es la distancia máxima posible entre la ubicación de la falla y el TP. El transformador más grande que fue elegido para las pruebas de CEPEL tuvo una distancia máxima entre el arco eléctrico y el TP de *8.5 metros (28'')* que corresponde casi a la mitad de la distancia máxima de un transformador de *750 MVA, 15 m (49'')*. Los resultados muestran la eficacia del TP incluso en estas condiciones críticas solamente con un Conjunto de Despresurización.

Study of the Pressure Wave Propagation and the Depressurisation Process for an Electrical Transformer Subjected to Internal Arcing

Design of a Decision-Making Management Tool for Transformer Explosion Prevention

Guillaume PERIGAUD (SERGI Holding Research Department Manager)
Héloïse CUNY (SERGI Holding Research Department Engineer)
Sylvain PRIGENT (SERGI Holding Development Department Manager)
Philippe MAGNIER (SERGI Holding CEO)
SERGI Holding, 186 av. du Général de GAULLE, 78260 ACHERES, FRANCE

Abstract

Oil-filled electrical transformers may be subjected to low impedance faults, which frequently result in the rupture of the transformer tank. SERGI designed and sells the TRANSFORMER PROTECTOR (TP) which prevents such dramatic events. In 2002 in order to prove the TP efficiency, Electricité de France (EDF) performed the first test campaign addressing arcing in a small transformer at its high voltage laboratory. The second campaign was performed in 2004 by CEPEL, the Brazilian high voltage laboratory. Tests were run on three industrial-sized transformers, each equipped with a TP. During the two campaigns, sixty-two tests were performed, all successful. The TP depressurised the transformer tanks and prevented the explosion each time. The tests thus experimentally proved the TP efficiency and reliability. Nevertheless, since every physical configuration cannot be tested, in 1995 SERGI developed a simulation tool, the MTH (Magneto-Thermo-Hydrodynamic) model. The MTH model numerically proved the TP reliability for various severe situations. This model has been upgraded to take into account very transient phenomena such as the pressure waves, their propagation inside the oil throughout the transformer, and their interaction with the tank structure. In the present article, which describes the updated modelling, oil and gas are considered compressible media. A full Eulerian compressible two-phase flow model is thus detailed in this article as well as the physical modelling assumptions. The thermodynamic characteristics for each medium are given. Various physical effects such as gravity, viscosity, heat transfers and arc influence on local pressure are modelled as well. A two-dimensional numerical tool is also presented: the geometry is split into smaller computational domains discretised by a structured mesh to account for the transformer complex geometry. The dedicated numerical methods to compute the different effects' contributions are also addressed. Riemann problem solvers, viscous, thermal, and gravity effects' numerical schemes are thus detailed. Particular attention is paid onto the numerical treatment of the boundary conditions, and especially on the TP numerical description and influence. Specific boundary conditions are set to accurately describe the TP. The advantages of such a method are recalled. The numerical tool capabilities are shown by a qualitative comparison between experimental and simulated pressure time evolutions regarding arcing tests performed at EDF. Both numerical and experimental pressure profiles are in good qualitative agreement. The pressure time evolution phases exhibited by the experiments are predicted by the simulation tool depending on the energy transferred by the arc to the oil. The complete quantitative study and the tool validation are not presented in this paper but are the important subject of another article [21]. The model and numerical method are able to accurately depict the pressure wave propagation and the TP influence is proved by the simulations.

Study of the Pressure Wave Propagation and the Depressurisation Process for an Electrical Transformer Subjected to Internal Arcing

Design of a Decision-Making Management Tool for Transformer Explosion Prevention

Guillaume PERIGAUD (SERGI Holding Research Department Manager)
Héloïse CUNY (SERGI Holding Research Department Engineer)
Sylvain PRIGENT (SERGI Holding Development Department Manager)
Philippe MAGNIER (SERGI Holding CEO)
SERGI Holding, 186 av. du Général de GAULLE, 78260 ACHERES, FRANCE

1. Introduction

In operation, the electrical transformers are cooled down by mineral or vegetable oil to avoid any kind of damage. It may occur that the oil loses its dielectric capabilities due to oil pollution or ionisation so that an electrical arc may occur. The electrical arc vaporises a part of the oil in its path and the created bubbles quickly grow and make a very sharp pressure rise. As the arc continues being fed, it breaks the oil into smaller molecules such as, carbon, hydrogen, or acetylene which is a highly flammable gas once in contact with air. The pressure rise generates pressure waves that propagate inside the oil and interact with the tank structure. This wave/structure interaction eventually leads to the tank rupture.

In order to prevent the tank rupture and the consequent huge facility losses [20] SERGI has designed an efficient transformer explosion prevention technology, the SERGI TRANSFORMER PROTECTOR (TP).

The TP efficiency to depressurise the transformer tank has been proved by two test campaigns [21]. Nevertheless, it seems technically impossible to experimentally illustrate extensively the TP efficiency on every geometry and every transformer type. Very few laboratories offer the various needed scientific warrantees, this type of tests requires, as well as the suitable infrastructures when dealing with transformer sizes about 10 to 15 meters, combined with a very high level of safety for facilities and persons. Moreover, the numerous types of transformers and their geometries prevent any systematic test policy because of their costs.

SERGI has thus undertaken a large research program since 1995, to create numerical decision-making and design tools. Numerical simulation enables indeed to have geometries, physical and electrical conditions easily and quickly varied and to check, step by step, that the TP is fully operational in any kind of configuration with time and money savings.

The MTH (Magneto-Thermo-Hydrodynamic) model [16] is operational since 1998 and showed the TP efficiency in many configurations [17][18][19]. Nonetheless it has recently been upgraded to describe the pressure wave propagation inside the tank. A suitable physical model associated with a reliable two-dimensional computational software was built in order to understand the physical phenomena involved in such a process and to avoid the difficulties of systematic experimentation campaigns.

This in-house developed simulation environment deals with two-phase flows. The physical mathematical set of partial differential equations governs the thermodynamic behaviour of the gas and liquid mixture, the pressure wave propagation, and the wave structure interaction with the complex geometries. It is thus based on robust numerical methods and a strong physical background.

The purpose of this article is thus to present the basis of the simulation tool, from a physical point of view as well as from a numerical one. The first section is dedicated to the physical modelling, the assumptions made, and the flow thermodynamics. The second section deals with the numerical method (numerical schemes), while in the third part, some numerical simulation results are displayed to show the model's ability to cope with the various and complex physical problems encountered with arcing inside oil-filled transformers.

2. Physical and Mathematical Modelling

2.1. Modelling Aims and Assumptions

The studied physical phenomena have very different features:

- Gases and liquids with their physical properties (viscosity, gravity, heat transfers);
- Violent pressure rises and pressure waves;
- Electrical arcs and their effect on the local pressure.

All previous aspects have to be accounted for in any modelling regarding transformer explosion prevention. Nevertheless some assumptions were done:

- The pressure is no longer considered spatially uniform (pressure wave propagation). The geometry influence on the simulation results is thus becoming more important than in the previous MTH version;
- The cracking chemical reactions are not accounted for because the harmful pressure waves to the tank structure are generated at the very first instant when the gas bubble appears. The vaporisation itself is sufficient to lead to the first pressure waves which will first interact with the tank structure and the TP;
- The mass transfer is implicitly taken into account when setting the initial conditions. Indeed, at the initial state:
  - The gas bubble is assumed to have already appeared and to already be under pressure ;
  - The arc energy transfer to the oil is assumed to be complete (100% of the electric energy is converted in overpressure), which overestimates the generated overpressure.

2.2. Bibliography

The model must describe compressible liquids. Similar models can be found in the literature. Most of the time, the compressible framework is used to depict liquids or solids when subjected to very high pressures. These pressure levels are encountered in the detonation field where pressures are so high that almost every material can be considered as a compressible medium.

Such an approach was used first by Baer & Nunziato [3] who derived the basis of a very general compressible two-phase flow model with two velocities and two pressures to depict explosions and detonations. Their work was modified, adapted, and improved, especially to take into account the relaxation terms to get back to mechanical equilibrium and deal with flows with interfaces [13] [15]. Some authors [10] modified the Baer & Nunziato model to describe the very complex physics involved inside deflagration and detonation phenomena in multi-material/multi-component flows. Other examples are seen in the literature, which describe the wave propagation inside liquids or solids by considering these media compressible [10][11][13].

Based on the general two-phase flow modelling exhibited in [3] , many authors simplified the equations to obtain an easier Partial Differential Equation (PDE) set to deal with. This was the case in [9] and [12] where an asymptotic analysis is used to simplify the general model assuming that the mechanical equilibrium must be fulfilled between phases in contact every time. This last model was simplified again to describe flows with gas/liquid interfaces, and has widely been studied in the literature: it proved its ability to accurately describe pressure wave propagation within two-phase flows [2][11][14].

The model which is hereafter detailed thus deals with two-phase flows by considering both phases compressible. The thermodynamics of both phases are carefully handled to avoid any theoretical problem and numerical oscillations. Our modelling is dedicated to flows with interfaces so that there is only one pressure and one velocity. Various physical effects (viscous, thermal, gravity effects, etc.) are also included.

2.3. Model Equations

The set of equations which is used to theoretically and numerically describe the phenomena is given by:

$$\begin{cases} \dfrac{\partial \alpha_1}{\partial t} + \vec{u}.\vec{\nabla}\alpha_1 = 0 \\ \dfrac{\partial \rho}{\partial t} + div(\rho\vec{u}) = 0 \\ \dfrac{\partial \alpha_1\rho_1}{\partial t} + div(\alpha_1\rho_1\vec{u}) = 0 \\ \dfrac{\partial \rho\vec{u}}{\partial t} + div(\rho\vec{u}\otimes\vec{u}+P) = \Phi_g^u + \Phi_\mu^u \\ \dfrac{\partial E}{\partial t} + div((E+P)\vec{u}) = \Phi_g^E + \Phi_\mu^E + \Phi_T^E + \dot{E} \end{cases} \quad \text{(eq. 1)}$$

$\alpha_1, \rho, \alpha_1\rho_1$ $\rho\vec{u}, P$, and E are respectively the gas volume fraction, the mixture density, the gas partial mass, the mixture momentum, the mixture pressure, and the mixture total energy.

The mixture density and mixture total energy expressions are respectively:

$\rho = \alpha_1\rho_1 + \alpha_2\rho_2$ and $E = (\alpha_1\rho_1\varepsilon_1 + \alpha_2\rho_2\varepsilon_2) + \frac{\rho\vec{u}^2}{2} = \rho\varepsilon + \frac{\rho\vec{u}^2}{2}$ where ε is the mixture internal energy.

$\Phi_g^{u,E}$, $\Phi_\mu^{u,E}$, and Φ_T^E stand respectively for gravity, viscosity, and heat conduction transfer contribution on momentum Φ^u and energy Φ^E equations. The source term $\dot{E}$ accounts for the arc energy transfer.

2.3.1. *Hydrodynamic Effects*

The hydrodynamic mathematical model is based on a set of PDE, which governs the hydrodynamic behaviour of mixtures. Thus it handles the two-phase flows between gases and liquids, and describes the oil as well as the gas bubbles generated by the arc. It consists of transport conservation laws for the mixture density, ρ, for the gas partial mass, $\alpha_1\rho_1$, for the mixture momentum, $\rho\vec{u}$, and the mixture total energy, E. The time evolution of the gas volume fraction, α_1, is governed by an advection equation which is no conservation law. One of the major and most interesting model's characteristics is its ability to accurately depict the pressure wave propagation inside liquids and gases. It is detailed in several references [2][11][14] and can be obtained from the general two-phase flow model described in [3] by an asymptotic analysis and an assumption on the volume fraction evolution [2][9][12]. Some physical effects are added in the modelling in order to be as close as possible to reality.

2.3.2. *Thermodynamic Closure*

Each fluid or phase has its own thermodynamic behaviour because it is described by its own Equation Of State (EOS). For the model to be complete and consistent, a thermodynamic closure has to be added in order to link the mixture pressure to the mixture total energy. Therefore an EOS is given for the whole mixture to deal with smeared interfaces between gas and oil due to numerical method diffusion.

2.3.2.1. *Stiffened Gas EOS*

This EOS [1][2][11][13] is very simple and robust. It only relies on two state parameters, the polytropic coefficient γ, and the stiffness parameter π. The behaviours of gases, liquids, and solids can be accurately described. The parameters are conveniently chosen to get the physical speed of sound in the media. Some examples are given in

Table 1.

Table 1: Stiffened Gas EOS Parameters.

	γ	Stiffness Parameter π		Speed of Sound c	
		10^8 *bar*	10^8 *Psi*	*m/s*	*ft/s*
Air	1.4	0	0	374	1227
Water (atmospheric)	4.1	4.4	64	1647	5403
Water (high pressure)	4	6	87	1820	5971
Oil	1.7	7	102	1200	3937
Copper	4.22	324	4698	3910	12828
Granite	2.2	142	2059	3750	12303

Fluid pressure and internal energy are thus linked by the following EOS:

$P = (\gamma - 1)\rho\varepsilon - \gamma\pi$ (eq. 2)

In the previous equation which links mixture pressure and mixture internal energy, the term $(\gamma - 1)$ corresponds to thermal expansion whereas $(-\gamma\pi)$ corresponds to the attractive effects inside the medium.

2.3.2.2. *State Parameters for Oil and its Vapour*

To accurately describe the pressure waves, the speed of sound is a very important parameter for the model to fit. The states parameters as well as other physical characteristics are set in Table 2 in order to get a modelled speed of sound that remains equal to the physical one.

Table 2 : Materials' Parameters for Oil and Its Vapour

			Oil Vapour	Oil
Polytropic Coefficient	γ		1.4	1.7
Stiffness Coefficient	π	(Pa)	0	$7\ 10^{8}$
Specific Heat Capacity	Cv	(J/kg)	$5\ 10^{2}$	$4\ 10^{3}$
Viscosity	μ	(Pa.s)	$20\ 10^{-6}$	10^{-3}
Thermal Conductivity	λ	($K.m^{-1}.K^{-1}$)	$2.62\ 10^{-2}$	$6\ 10^{-1}$

2.3.2.3. Mixture "Stiffened Gas" EOS

Due to pressure equilibrium, a mixture "Stiffened Gas" EOS is built involving two mixture state parameters γ, and π. These are functions of each fluid state parameters and volume fractions:

$$\gamma = \frac{\dfrac{\alpha_1\gamma_1}{\gamma_1-1}+\dfrac{\alpha_2\gamma_2}{\gamma_2-1}}{\dfrac{\alpha_1}{\gamma_1-1}+\dfrac{\alpha_2}{\gamma_2-1}} \quad \text{and} \quad \pi = \frac{\dfrac{\alpha_1\gamma_1\pi_1}{\gamma_1-1}+\dfrac{\alpha_2\gamma_2\pi_2}{\gamma_2-1}}{\dfrac{\alpha_1\gamma_1}{\gamma_1-1}+\dfrac{\alpha_2\gamma_2}{\gamma_2-1}}$$

This mixture EOS is very useful to handle the artificial mixture zone generated between liquids and gases by the model evolution.

A mixture specific heat capacity at constant volume, and a mixture temperature can be defined as:

$$C_v = \sum_k \alpha_k \rho_k C_{vk} \quad \text{(eq. 3) and } T = \frac{\sum_k \alpha_k \rho_k C_{vk} T_k}{\sum_k \alpha_k \rho_k C_{vk}} \quad \text{(eq. 4)}$$

where, as each fluid k is governed by a "Stiffened Gas EOS", and where:

$$T_k = \frac{P+\pi_k}{\rho_k C_{vk}(\gamma_k - 1)}$$

More details can be found in the literature [1][2][11][13][14][15] which show the ability of the method to describe the pressure wave propagation in two-phase flows.

2.3.3. Gravity Effects, Viscous and Thermal Effects

In the equation (1) the various terms Φ_g^u, Φ_g^E, Φ_μ^u, Φ_μ^E and Φ_T^E have the following forms:

$$\Phi_g^u = \rho\vec{u}\ ,\ \Phi_g^E = \rho\,\vec{u}.\vec{g}\ ,\ \Phi_\mu^u = div\left(\mu\overline{\overline{\tau}}\right),\ \Phi_\mu^E = div\left(\mu\overline{\overline{\tau}}.\vec{u}\right), \text{ and } \Phi_T^E = \sum_k \alpha_k\, div\left(K_k \vec{\nabla} T_k\right)$$

Where:

μ is the mixture viscosity defined as $\mu = \alpha_1\mu_1 + \alpha_2\mu_2$ with μ_k the dynamic viscosity for phase k,

K_k and T_k are respectively the heat conductivity and the phase temperature for phase k.

Finally, the viscous mixture stress tensor, $\overline{\overline{\tau}}$, has the following form:

$$\overline{\overline{\tau}} = -\frac{2}{3} div(\vec{u})\overline{\overline{I}} + 2\overline{\overline{D}} \quad \text{(eq. 5)}$$

$\overline{\overline{D}}$ is the deformation rate tensor defined as $\overline{\overline{D}} = \frac{1}{2}\left(\overline{\overline{grad}}\ \vec{u} + \overline{\overline{grad}}^{\,t}\ \vec{u}\right)$, with $\left[\overline{\overline{grad}}\ \vec{u}\right]_{ij} = \frac{\partial u_i}{\partial x_j}$.

2.3.4. Arc Energy Transfer

The modelling of the arc energy transfer is very important to solve the problems we are interested in. The following sections regard the expression of the energy source term $\dot{E}$.

2.3.4.1. Symmetrical Current

The arc influence is of utmost importance in our case. The modelling takes into account the energy transfer from the arc to the oil. We assume that the energy transfer is 100% efficient so that no energy loss is accounted for.

This transfer results in a local pressure rise which is governed by the energy source term $\dot{E}$:

$\dot{E} = W \times H_{\chi}(\underline{x},t)$ (eq. 6)

Where W is the instantaneous electrical arc power, and $U(t)$ the electrical arc voltage. The mathematical function $(\underline{x},t) \rightarrow H_{\chi}(\underline{x},t)$ is the arc test function defined as follows:

$$H_{\chi}(\underline{x},t) = \begin{cases} 1 \text{ if } \underline{x} \in \chi \text{ and } t < \Delta T \\ 0 \text{ else} \end{cases} \quad \text{(eq. 7)}$$

The current $I(t)$ is assumed sinusoidal ($I(t) = I_{\max} \sin(2\pi ft)$) so that power reads $W = U(t) I_{\max} \sin(2\pi ft)$, and $U(t)$ is a square wave signal based on current sign and whose amplitude is $U_{\max}$. $I(t)$, and $U(t)$ are in phase. The maximum voltage values are randomly disturbed up to 15% in order to account for the arc random behaviour. The result of this strategy is illustrated in Figure 1. ΔT stands for the arc duration.

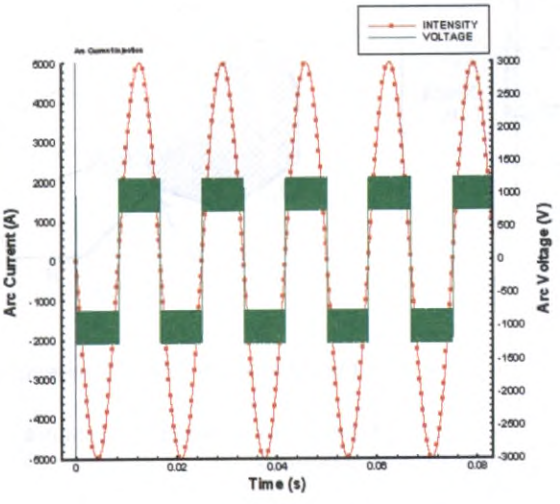

Figure 1 : Symmetric Simulated arc Current and Voltage

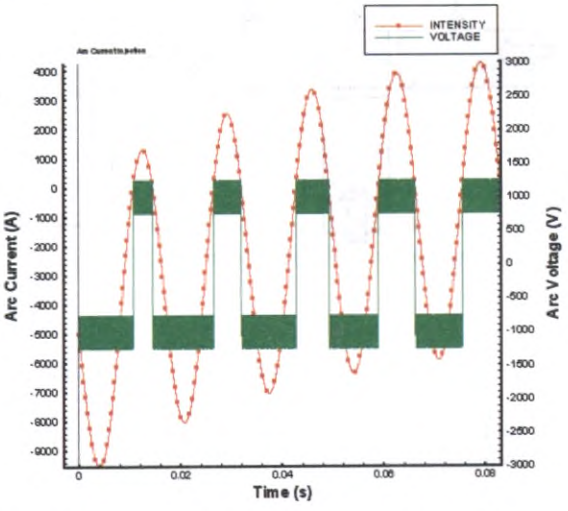

Figure 2 : Asymmetric Simulated Arc Current and Voltage

2.3.4.2. Asymmetrical Current

During the CEPEL experiments, the current symmetry has been broken in order to maximise the energy injected and transferred to the oil and thus to increase the pressure peak level.

Numerically, an "asymmetrisation" procedure has been set up by adding an exponential component whose variable is the arc feeding duration. The analytical expression of this addition is the following:

$$I(t) = \Delta I \times e^{-\frac{2t}{\Delta t_{arc}}} - I_{nom} \times \sin(2\pi ft) \quad \text{(eq. 8)}$$

Where $\Delta I = I_{\max} - I_{nom}$ and $I_{\max}$ is the current maximum value, while I_{nom} is the nominal current value for the test. The electric profiles are thus modified as shown on Figure 2.

3. Numerical Methods

3.1. Simplifications

Several approximations were done to numerically simulate the transformer explosion prevention by the TP. These assumptions regard the following points:

- The geometry of the problem is reduced to a two-dimensional geometry without any major influence on the results liability;
- The transformer is split into elementary calculation blocks whose shape can be deduced by applying bijective functions to any rectangle. Each of them is discretised by a structured mesh as shown in the following;
- The windings and the magnetic transformer core are modelled by a rigid obstacle which interacts with the pressure waves;

- The oil/structure mechanical coupling is weak, which strengthens the TP operation conditions because all the energy transferred from the arc to the oil is converted into overpressure and not dissipated into mechanical energy by the wall elasticity;
- The OGST (Oil and Gas Separation Tank) and the Decompression Chamber are not numerically simulated. The Decompression Chamber is taken into account due to the subsonic inlet/outlet boundary conditions.

3.2. 2D Finite Volume Method and Multi-Block Geometry Description

In order to perform numerical simulations, the physical geometry has to be split into smaller sub-domains called blocks, which are then spatially discretised. These resulting meshes are thus made of small calculation cells where physical variables are assumed to be constant.

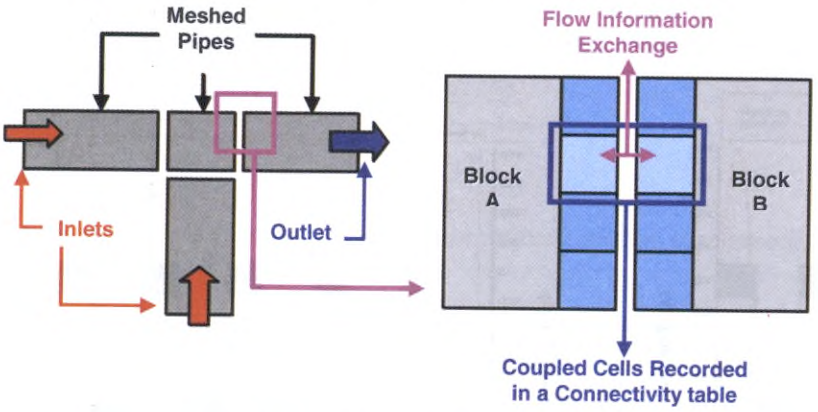

Figure 3 : Example of a Multi-Block Strategy and Connectivity Table

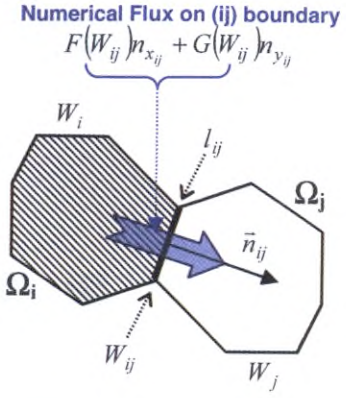

Figure 4: Mesh Cell & Parameters

We adopt a Finite Volume Method to numerically solve the PDE's system . A multi-block strategy is retained and connectivity tables are created in order to make neighbouring blocks exchange information.

3.3. Numerical Schemes

The model under consideration in the present study is based on a hyperbolic hydrodynamic model for compressible two-phase flows [2][11][14] where various physical effects are included (viscosity, heat transfers, gravity, other energy transfers). A numerical scheme and method is thus associated with every effect.

3.3.1. Hydrodynamic Numerical Schemes

The hydrodynamic part of the equations is the most important part of the modelling because the pressure waves are depicted by this part of the equations. The model can be written in the following compact form:

$$\begin{cases} \dfrac{\partial \alpha}{\partial t} + \vec{u}.\vec{\nabla}\alpha = 0 \\ \dfrac{\partial W}{\partial t} + \dfrac{\partial F(W)}{\partial x} + \dfrac{\partial G(W)}{\partial y} = 0 \end{cases} \quad \text{(eq. 9)}$$

Where $W^t = [\alpha_1, \rho, \alpha_1\rho_1, \rho u, \rho v, E]$

and

$F(W) = [0, \quad \rho u, \quad \alpha_1\rho_1 u, \quad \rho u^2 + P, \quad \rho uv, \quad (E+P)u]$ (eq. 10)

$G(W) = [0, \quad \rho v, \quad \alpha_1\rho_1 v, \quad \rho uv, \quad \rho v^2 + P, \quad (E+P)v]$ (eq. 11)

This model can be divided into two parts, one conservative, and the other non conservative.

In both cases, the Finite Volume Method is used to find the suitable discretisations as explained hereafter.

3.3.1.1. PDE Model Analysis

As for every PDE system we can associate a Jacobian Matrix to the set of equation. The matrix associated with our PDE system once projected on the local coordinate system is thus:

$$A_n(Y)=R^t\left(n_x.(A(W)+C_x(W))\frac{\partial W}{\partial x}+n_y.(B(W)+C_y(W))\frac{\partial W}{\partial y}\right)R=\begin{pmatrix} u_n & 0 & 0 & 0 & 0 & 0 \\ 0 & u_n & 0 & \rho n_x & \rho n_y & 0 \\ 0 & 0 & u_n & \alpha_1\rho_1 n_x & \alpha_1\rho_1 n_y & 0 \\ 0 & 0 & 0 & u_n & 0 & \frac{n_x}{\rho} \\ 0 & 0 & 0 & 0 & u_n & \frac{n_y}{\rho} \\ 0 & 0 & 0 & \rho c^2 n_x & \rho c^2 n_y & u_n \end{pmatrix} \quad \text{(eq. 12)}$$

Where $Y^t=[\alpha_1,\rho,\alpha_1\rho_1,u,v,P]$ is the non conservative variable set, $A(W)=\frac{\partial F(W)}{\partial W}$ and $B(W)=\frac{\partial G(W)}{\partial W}$ are the Jacobian Matrixes in both x and y directions, $C_x(W)$, $C_y(W)$ are the non conservative term matrices, and R is the orthogonal change-of-basis matrix from W -basis to Y -basis.

The PDE system analysis can then be performed on this matrix to find the mathematical properties of the physical model. The eigenvalues are of utmost importance in that kind of problems. In our case they are:

$$\lambda_1=u-c$$
$$\lambda_2=u \quad \text{(eq. 13)}$$
$$\lambda_3=u+c$$

It can be shown that λ_1 and λ_3 are acoustic waves (typically rarefaction waves and shocks), whereas λ_2 is a contact discontinuity. Their orders of multiplicity are, respectively, 1, 4, and 1. The associated Riemann problem is thus very similar to the one associated with Euler equations [6][8][23]. The corresponding right eigenvectors can be calculated:

$$R_1^t=[0,\rho,\alpha_1\rho_1,-cn_x,-cn_y,\rho c^2]$$
$$R_{21}^t=[1,0,0,0,0,0],\ R_{22}^t=[0,1,0,0,0,0],\ R_{23}^t=[0,0,1,0,0,0],\ R_{24}^t=[0,\ 0,0,-n_y,n_x,\ 0] \quad \text{(eq. 14)}$$
$$R_3^t=[0,\rho,\alpha_1\rho_1,cn_x,cn_y,\rho c^2]$$

A more detailed analysis shows that the dimensions of the eigenspace associated with every eigenvalue is equal to the eigenvalue's multiplicity, which means that the PDE system is hyperbolic and can be numerically solved using the usual dedicated numerical methods. The previous eigenvectors are very important because Riemann solvers can be built to compute numerical fluxes at each cell boundary, as explained in section 3.4.

3.3.1.2. *Finite Volume Scheme for the Conservative Part*

We consider system (eq. 1) where W is defined as in expression (eq. 9). Moreover, let us note:

$$\Psi(W)=[F(W)|G(W)]$$

We then apply a Finite Volume Method onto the system (eq. 9):

$$\int_{\Omega_i}\int_{\Delta t}\frac{\partial W}{\partial t}d\Omega dt+\int_{\Omega_i}\int_{\Delta t}\frac{\partial F(W)}{\partial x}d\Omega dt+\int_{\Omega_i}\int_{\Delta t}\frac{\partial G(W)}{\partial y}d\Omega dt=0$$

The numerical scheme for the conservative part of the hydrodynamic model finally reads:

$$\Omega_i\left(W_i^{n+1}-W_i^n\right)+\Delta t\sum_{j\in V(i)}\left(F\left(W_{ij}^n\right)n_{x_{ij}}+G\left(W_{ij}^n\right)n_{y_{ij}}\right)l_{ij}=0 \quad \text{(eq. 15)}$$

$$\Omega_i\left(W_i^{n+1}-W_i^n\right)+\Delta t\sum_{j\in V(i)}\Psi\left(W_{ij}^n\right)\vec{n}_{ij}l_{ij}=0 \quad \text{(eq. 16)}$$

The quantity $\Psi(W_{ij}).\vec{n}_{ij}=F\left(W_{ij}\right)n_{x_{ij}}+G\left(W_{ij}\right)n_{y_{ij}}$ is the numerical flux at the cell boundary between cell i and cell j. It has to be evaluated at each cell-boundary.

3.3.1.3. *Finite Volume Scheme for the Non Conservative Part*

In addition to the conservative part of the equations, the gas volume fraction behaves according to an advection equation. Several ways to handle such terms are noted in the literature, but the Godunov numerical scheme for an advection equation has been preferred to solve our problem:

$$\alpha_i^{n+1} = \alpha_i^n - \frac{\Delta t}{\Omega_i} \sum_{j \in V(i)} \left(\alpha_{ij}^n - \alpha_i^n\right) \vec{u}_{ij}^n . \vec{n}_{ij} \, l_{ij} \quad \text{(eq. 17)}$$

This discretisation scheme is very numerically robust and stable, and is retained for our applications.

3.3.2. *Gravity, Viscous and Thermal Effects, and Arc Energy Transfer*

φ is any of the physical variables. We note φ^* any intermediate temporal state between the two instants n and $n+1$, solution of a time dependant PDE including the contributions of the physical effects considered separately.

3.3.2.1. *Gravity*

The gravity source terms are taken into account by a time splitting scheme as showed by:

$$\frac{\partial W}{\partial t} = \Phi_g(W) \quad \text{(eq. 18)}$$

Where $W^t = [\alpha_1, \rho, \alpha_1\rho_1, \rho u, \rho v, E]$ and $\Phi_g^t = [0, 0, 0, \rho g_x, \rho g_y, \rho \vec{u}.\vec{g}]$.

The resulting numerical scheme based on a first order Runge-Kutta time scheme, is thus the following:

$$\alpha_i^* = \alpha_i^n, \; \rho_i^* = \rho_i^n, \; (\alpha_1\rho_1)_i^* = (\alpha_1\rho_1)_i^n, \; u_i^* = u_i^n + \Delta t . g_x, \; v_i^* = v_i^n + \Delta t . g_y, \; E_i^* = E_i^n + \rho_i^n \Delta t \left(g_x . u_i^n + g_y . v_i^n\right)$$

3.3.2.2. *Viscous and Thermal Effects*

The contribution of the viscous and the thermal effects is obtained proceeding the same way as for the hydrodynamic part. The associated numerical scheme is thus:

$$W_i^* = W_i^n + \frac{\Delta t}{\Omega_i}\left(\left(\Phi_\mu\right)_i^n + \left(\Phi_T\right)_i^n\right) = W_i^n + \frac{\Delta t}{\Omega_i} \begin{pmatrix} 0 \\ 0 \\ 0 \\ \displaystyle\sum_{j \in V(i)} \mu_{ij}^n \overline{\overline{\tau}}_{ij}^{=n} . \vec{n}_{ij} l_{ij} \\ \displaystyle\sum_{j \in V(i)} \mu_{ij}^n \left(\overline{\overline{\tau}}_{ij}^{=n} . \vec{u}_{ij}^n\right) \vec{n}_{ij} l_{ij} + \sum_k \alpha_{ki}^n \sum_{j \in V(i)} \left(K_k \vec{\nabla} T_k^n\right)_{ij} . \vec{n}_{ij} l_{ij} \end{pmatrix} \quad \text{(eq. 19)}$$

The velocity gradients $\left(\overline{\overline{grad\,\vec{u}}}\right)_{ij}$ and consequently the viscous stress tensor $\overline{\overline{\tau}}_{ij}$ as well as the dynamic viscosity μ_{ij} are evaluated at each cell boundary. The evaluation method is the one used in [22]. The temperature gradients $\left(\vec{\nabla} T_k\right)_{ij}$ are evaluated the same way as the velocity gradients are. Note that here we do not work with the mixture temperature to compute thermal contributions due to heat conduction

3.3.2.3. *Arc Energy Transfer*

The arc energy source terms are taken into account by a time splitting scheme:

$$\frac{\partial W}{\partial t} = \Phi_{\dot{E}}(W) \quad \text{(eq. 20)}$$

Where $W^t = [\alpha_1, \rho, \alpha_1\rho_1, \rho u, \rho v, E]$ and $\Phi_{\dot{E}}^t = [0, 0, 0, 0, 0, \dot{E}]$.

The resulting numerical scheme based on a first order Runge-Kutta time scheme, is thus the following:

$$\alpha_i^* = \alpha_i^n, \; \rho_i^* = \rho_i^n, \; (\alpha_1\rho_1)_i^* = (\alpha_1\rho_1)_i^n, \; u_i^* = u_i^n, \; v_i^* = v_i^n, \; E_i^* = E_i^n + \Delta t . \dot{E}\left(\underline{x_i}; \chi_{arc}\right)$$

Where $\underline{x_i}$ is the cell gravity centre and χ_{arc} is the arc support which accounts for the arc influence zone.

3.4. *Riemann Problems and Solvers*

3.4.1. *Riemann Problem*

A Riemann problem consists of a Partial Differential Equation (PDE) set whose initial conditions are uniform on both sides of an initial single discontinuity. Time evolution of such problems can be described when introducing the wave concept. Details about Riemann problems, their adaptation, and their solving can be found in [7][8][23].

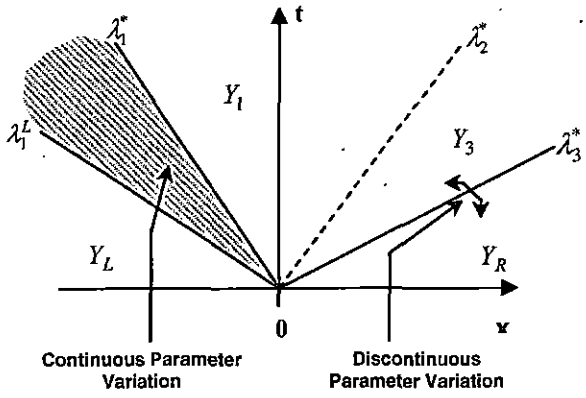

Figure 5 : Riemann Problem Illustration

3.4.2. Riemann Solvers

In fact, at every time step in a Finite Volume Method, since all variables are constant on one given cell, there is a variable discontinuity at cell boundaries. In order to find the appropriate values of the variables at each cell boundary, a Riemann problem has to be solved at every cell boundary using dedicated Riemann solvers in order to correctly evaluate all adequate variables noted W_{ij} the cell interfaces for the numerical flux computation, $\Psi(W_{ij})\vec{n}_{ij}$. These values are the solution of the Riemann problem between cell Ω_i and cell Ω_j. Dedicated Riemann solvers thus exist and are divided in three mains categories: Some exactly solve an exact Riemann problem (Godunov Solver [8][23]), others solve an approximate Riemann problem (VFRoe [6], or acoustic solvers [23]), while the last approximately solve an approximate Riemann problem (Roe, Rusanov [4]). For more details on this particular subject, references [6][8][23] would be of great interest.

A Riemann solver that exactly solves the exact Riemann problem has been built for the model we work with. Following the rules detailed in [23] when presenting the Godunov solver for Euler equations we can also build an exact solver for our model. The various state expressions can be deduced from the ones in [23] and are not recalled in the present document. When dealing with a numerical tool this solver has be associated with numerical schemes and boundary treatment.

3.5. Boundary Conditions

The boundary conditions are some of the cornerstones of the numerical tool under consideration. They are accounted for by virtual cells neighbouring cells located at the very limit of the geometry profile (cf. Figure 6).

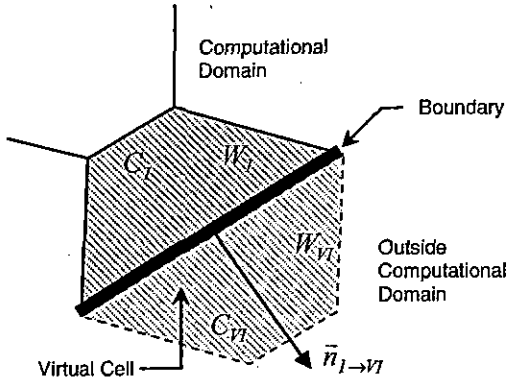

Figure 6 : Boundary Cell and its Associated Virtual Cell

The variables in those virtual cells are set depending on the type of boundary conditions one has imposed. Once those cells are updated with new variables, one can solve a Riemann problem at the edge, between the cell and the boundary, in order to compute a numerical flux.

Several types of boundary conditions are considered in the present work. They are detailed hereafter.

3.5.1. *Imposed Boundary Conditions*

In this case, the virtual cell is set with a reference state, which remains constant from time step to another.

3.5.2. *Absorption Boundary Conditions*

In this case, the virtual cell is set with the current state of the neighbouring cell inside the physical domain; the current inner state is actually copied into the virtual cell.

3.5.3. *Slipping and No-Slipping Wall Boundary Conditions*

In the following U_n is the normal velocity to the wall evaluated at the wall and U_t is the tangential velocity to the wall evaluated at the wall as well. The virtual state is set such as the fluid cannot go through the boundary, which means $U_n = 0$. To achieve such a goal, and knowing the inner domain state $W_I = (\alpha_I, \rho_I, \alpha_{1I}\rho_{1I}, U_{nI}, U_{tI}, P_I)^t$, the virtual state is defined as follows:

$$W_{VI} = (\alpha_I, \rho_I, \alpha_{1I}\rho_{1I}, -U_{nI}, U_{tI}, P_I)^t$$

If viscosity effects are taken into account, the velocity at the wall must be zero:

$$W_{VI} = (\alpha_I, \rho_I, \alpha_{1I}\rho_{1I}, -U_{nI}, -U_{tI}, P_I)^t$$

3.5.4. *Automatic Subsonic Inlet/Outlet Boundary Conditions*

We can see in Figure 7 and Figure 8 below, only two waves out of three are located on the same side of the boundary so that the virtual state is not simple to determine. We recall that the normal vector to the boundary always heads outward the physical domain.

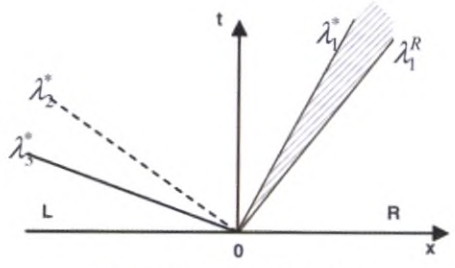

Figure 7 : Subsonic Inlet

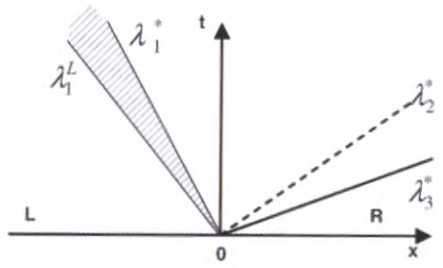

Figure 8 : Subsonic Outlet

In order to get analytical expressions easily handled in a calculation or by CFD codes, it is assumed that shocks can be described by an isentropic compression [5].

The sought state is noted φ^*. Then, one of the boundary cell edge variables is set arbitrarily - most of the time the pressure p^* is - and the Riemann invariants across the different waves are combined to get the sought parameters. For the present model, the Riemann invariants read (subscript φ_I stands for the inner computational domain variables, and the subscript φ_0 for the state reference):

- **For a subsonic outlet:**

$$p^* = p_{imposed},\ \alpha^* = \alpha_I,\ \rho^* = \rho_I\left(\frac{p^* + \pi(\alpha^*)}{p_I + \pi_I}\right)^{\frac{1}{\gamma(\alpha^*)}},\ \rho_g{}^* = \rho_{gI}\left(\frac{p^* + \pi(\alpha^*)}{p_I + \pi_I}\right)^{\frac{1}{\gamma(\alpha^*)}},\ U_n{}^* = U_{nI} + 2\frac{c_I - c^*}{\gamma_I - 1},\ U_t{}^* = U_{tI}$$

(eq. 21)

- **For a subsonic inlet:**

$$p^* = p_{imposed} \neq p_0,\ \alpha^* = \alpha_0,\ \rho^* = \rho_0\left(\frac{p^* + \pi(\alpha^*)}{p_0 + \pi_0}\right)^{\frac{1}{\gamma(\alpha^*)}},\ \rho_g{}^* = \rho_{g0}\left(\frac{p^* + \pi(\alpha^*)}{p_0 + \pi_0}\right)^{\frac{1}{\gamma(\alpha^*)}},\ U_n{}^* = U_{n0} - 2\frac{c_0 - c^*}{\gamma_0 - 1},\ U_t{}^* = U$$

(eq. 22)

Note that we use the inner pressure and an imposed external state to calculate respectively the outlet and inlet virtual states.

3.5.5. *TRANSFORMER PROTECTOR (TP) Boundary Conditions*

The Rupture Disk (RD) behaviour is essential in the transformer tank depressurisation process. The RD opening was experimentally studied in details during the 2002 EDF test and 2004 CEPEL test campaigns.

3.5.5.1. *Experimental TP behaviour*

The two experimental test campaigns, respectively carried out by EDF and by CEPEL, showed that:

- The TP begins to react significantly to the pressure rise once the calibrated pressure in the TP vicinity is over the calibrated pressure ;
- The TP begins to open approximately two or three milliseconds after having detected the significant overpressure (structural inertia, RD bulge before rupture) ;
- The RD opening is complete after 10 ms.

The numerical modelling of the TP has thus to account for these physical observations.

3.5.5.2. *TP Modelling Assumptions*

The TP reacts to the overpressure as soon as the pressure in the calculation cell neighbouring the TP location reaches the pressure threshold that is the calibrated pressure. The RD begins thus to open 3 ms after that first detection. The TP opening characteristics are thus:

- The opening is concentric (axis symmetry);
- The opening is progressive:
  - In three phases which last 3 ms each;
  - All boundaries that describe the same TP part of one considered phase open simultaneously.

3.5.5.3. *TP Boundary Numerical Treatment*

The TP is described by three zones, each corresponding to one colour. The three colours which enable to manage the three previously mentioned phases are arbitrary set to 35 (first phase), 335 (second phase), and 3335 (last phase). These three phases behave the same way but are each delayed of a few milliseconds. As long as the RD calibrated pressure is not reached in any boundary cell adjacent with the TP, the boundary edges whose colour is 35, 335, or 3335 behave as if they were walls. Therefore, the virtual boundary states used to manage the boundary conditions are set with the virtual states corresponding to walls.

At every time step, a test on the wall-pressure checks whether the pressure in any 35, 335 or 3335-coloured cell has reached the RD calibrated pressure, P_c. If this condition is true, a tempo is activated and measures 3 ms. During that duration, all boundaries associated with the TP are considered walls. Once the 3 ms elapsed, the 35-coloured cells, located at the TP centre open, all at once. The 335-coloured cells open then 3 ms later and the last part of the TP, the 3335-coloured cells, open 3 ms later at their turn. The full opening, composed of 3 phases lasts 9 ms from the moment when the significant overpressure is detected as shown in Figure 9.

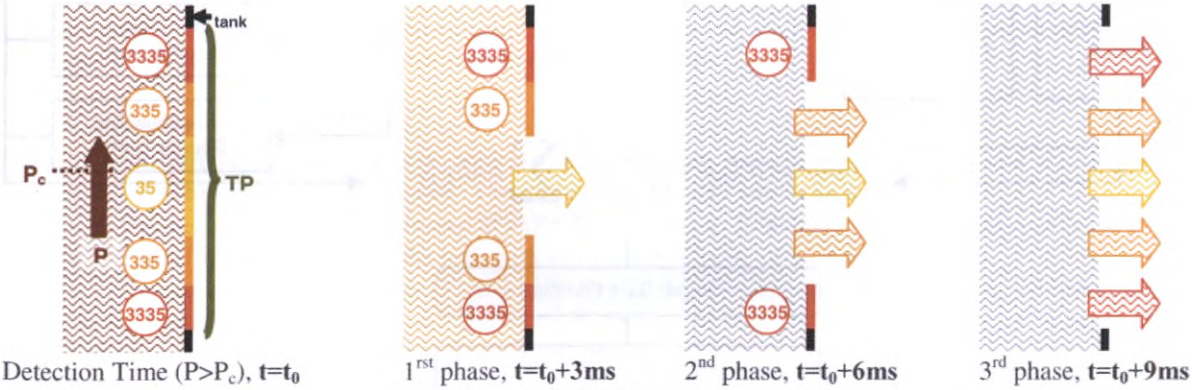

Figure 9 : TP Opening Phases

Once elapsed each phase's delay, TP boundaries are only considered subsonic inlets/outlets and no longer walls.

Reference physical states, set before the calculation begins, are the information needed to solve the Riemann problems at these boundaries. The pressure outside the transformer is usually set as a reference state for the computation:

- P_{ref}=1bar (14.5 psi) when the Oil and Gas Draining Pipe and the OGST (Oil and Gas Separation Tank) are under atmospheric pressure (standard TP operation conditions);
- P_{ref}=0.1bar (1.45 psi) when the pipes are under vacuum.

3.6. *Advantages of the Modelling*

The previous modelling advantages are numerous. The main ones are recalled hereafter:

- Complex geometries can be easily simulated;
- Each fluid is described by its own EOS and its own state parameters;
- The model deals with compressible two-phase flows, and in particular with gas/liquid interface flows;
- Liquid compressibility is taken into account very accurately so that pressure wave propagation inside liquids can be studied in detail;
- This very general model handles complex physics such as two-phase viscous effects, two-phase heat conduction, gravity, and mass transfer;
- The model is valid whatever the location in the flow: the equations stand for pure fluids as well as for interface vicinity;
- The model equations are very simple and can be numerically solved more easily than other physical models. The corresponding numerical methods are also much simpler than some other used to simulate the same type of two-phase flow problems.

3.7. *Simulation Procedure Diagram*

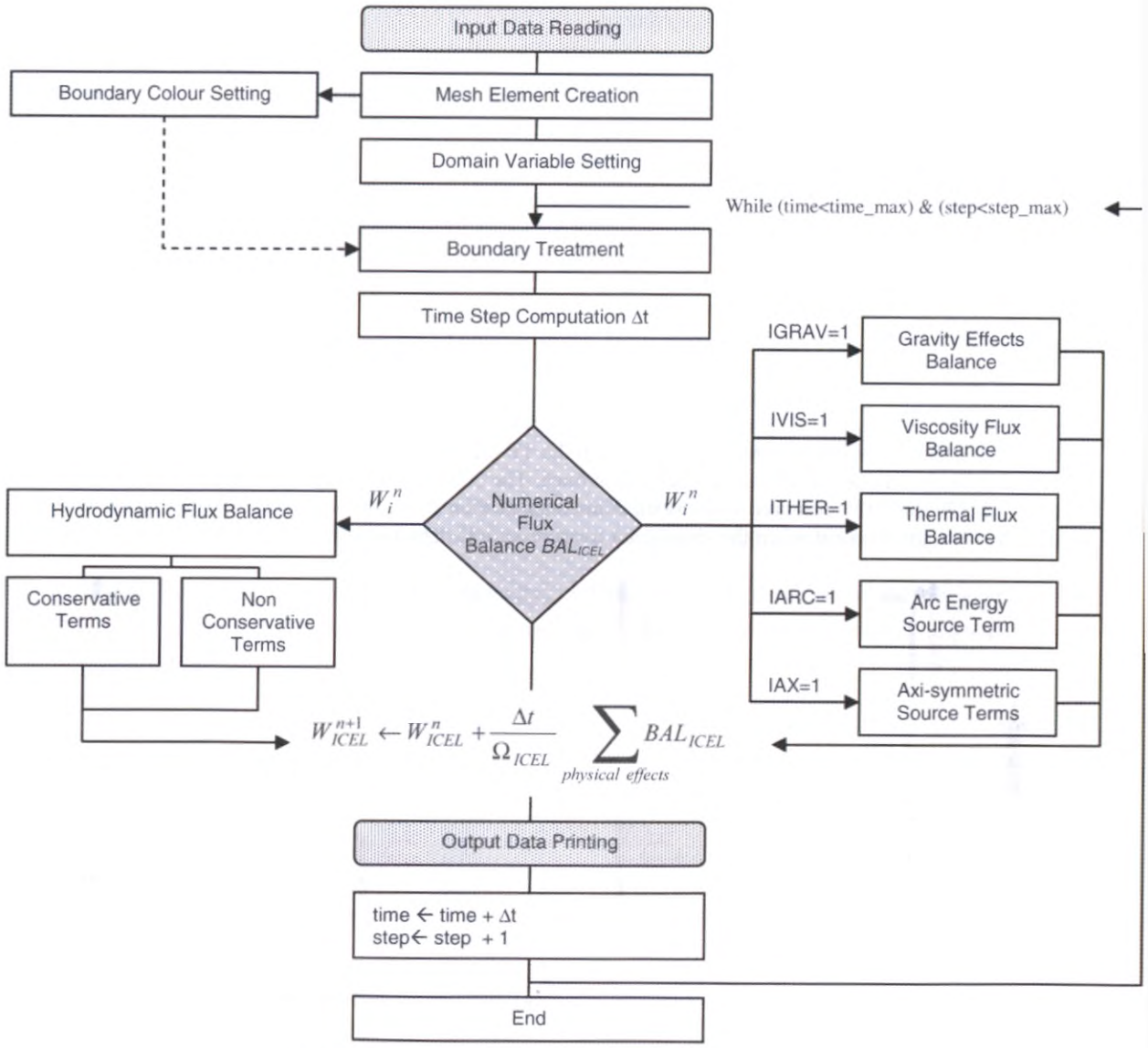

Figure 10: Numerical Tool Logical Diagram

4. Simulation Tool Capabilities Illustration – Electricité de France (EDF) tests (2002)

The purpose of this section is more to show the numerical tool ability to simulate our physical problems than to quantitatively validate it. The following study is thus focused on the numerical tool's qualitative behaviour and

on its ability to accurately describe the pressure wave propagation. Nevertheless, the validation of the numerical tool is studied in details in the article [21].

4.1. Presentation

In 1995 SERGI launched an ambitious research program, in order to acquire a better knowledge of the phenomena that lead a transformer to explode. The MTH (Magneto-Thermo-Hydrodynamic) model was developed to simulate the occurrence of a fault inside a transformer and the tank depressurisation by the TRANSFORMER PROTECTOR (TP). In 2002, SERGI performed 28 experimental tests on a 0.16 MVA transformer tank at Extra High Voltage Laboratory of Electricité de France (EDF), to validate the results of the MTH model and prove the TP efficacy in harsh conditions of electrical arcs caused by a low impedance fault.

4.2. Experimental Tests

4.2.1. Overview

The test bench displayed in Figure 11 is composed of a 109 litre tank (similar to the tank of a 0.16MVA transformer), feeding electrodes, and a Buchholz relay.

The tank is equipped with a standard TP.

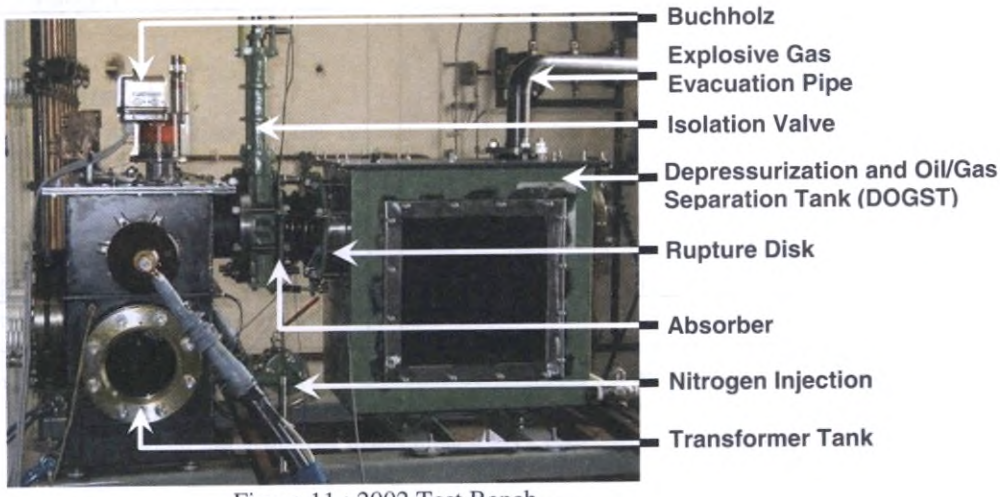

Figure 11 : 2002 Test Bench

Viewing windows were mounted on the transformer tank and on the DOGST to observe several phenomena such as arc creation, bubble growth, depressurisation and oil jet. In addition, electrical measurements (current, voltage, secondary arc…) and pressure evolution were recorded.

4.2.2. Results

The 28 tests were successful. The tank, subjected to very strong stresses, did not rupture and was depressurised by the TP, preventing any tank explosion. The study of the 28 tests shows us that:

- The tank inner pressure increased at a rate of 250 bar/s to 1200 bar/s (3625 to 17400 psi/s) ;
- The oil was expelled from the tank with an average velocity of 16.8 m/s (51ft/s);
- The pressure peaks of 2.5bar (37 psi) to 7.5 bar (109 psi) were experimentally obtained inside the tank.

Two tests, whose pressure profiles are presented in Figure 12 and Figure 13, are selected because they are representative of different types of behaviour (Table 3).

Table 3: Test Characteristics

Test	20	27	**Test**	20	27
Maximum Current	5000 A	5000 A	**Arc Energy**	162.7 kJ	127.8 kJ
Arc Duration	80 ms	80 ms	**Maximum Pressure**	4 bar (58 Psi)	3.5 bar (50.75 Psi)
Energy at 10ms	16.54 kJ	10.06 kJ	**Pressure Gradient**	610 bar/s (8800 Psi/s)	550 bar/s (8000 Psi/s)

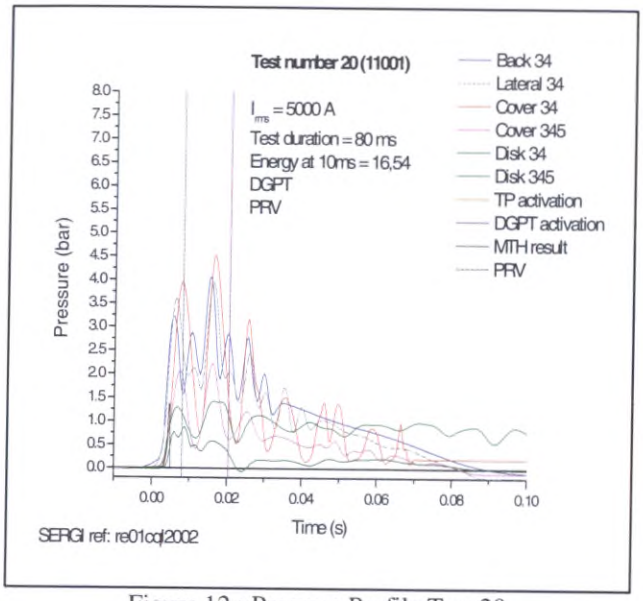

Figure 12 : Pressure Profile Test 20

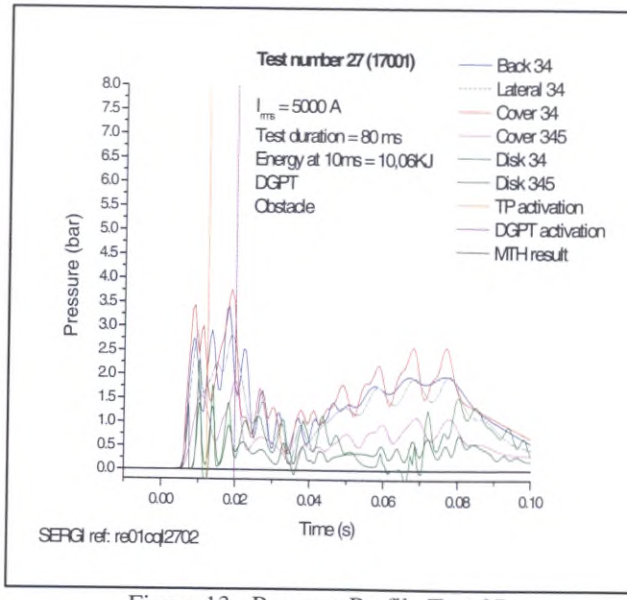

Figure 13 : Pressure Profile Test 27

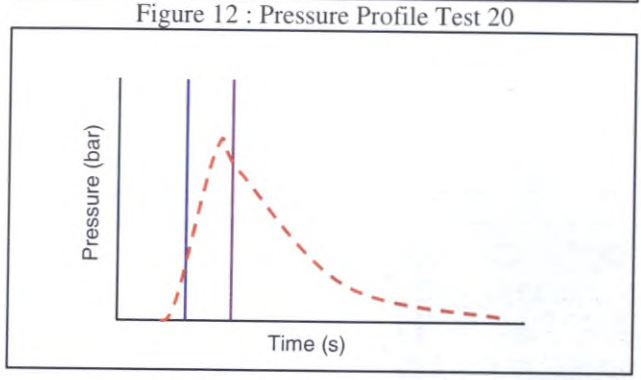

Figure 14 : Pressure Trend, Test 20

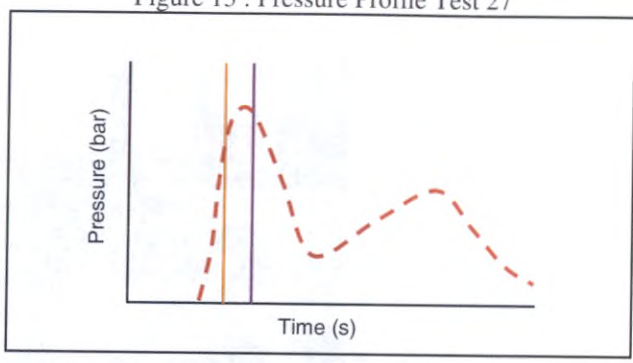

Figure 15 : Pressure Trend, Test 27

These tests are very interesting because they give a example of two different pressure behaviours.

- Test 20 : The gas bubble creation marks the beginning of a phase of pressure increase, followed by a decompression phase until the inner pressure is back to the atmospheric one (Figure 14).
- Test 27 : The compression phase is also followed by a depressurisation phase, however, before the inner pressure is back to the atmospheric one, a new compression can be noticed followed by a final depressurisation (Figure 15).

The following numerical comparison was made with these two tests as reference.

4.3. Numerical Tests

4.3.1. Geometry

The simulation environment deals with two-dimensional geometries. So, to find a compromise between experiments and the needs involved by a modelling, we use the plane of symmetry of the tank, and we reduce the study space to the median plane of these tank. The chosen geometry and its dimensions are specified in Figure 16 that gives information on the splitting in 4 blocks, used to build any calculation on these tests. The details of the discretisation are summed up in Table 4.

Table 4 : Discretisation Details

Block	Number of points	
	Direction x	Direction y
1	31	34
2	31	17
3	31	4
4	9	17

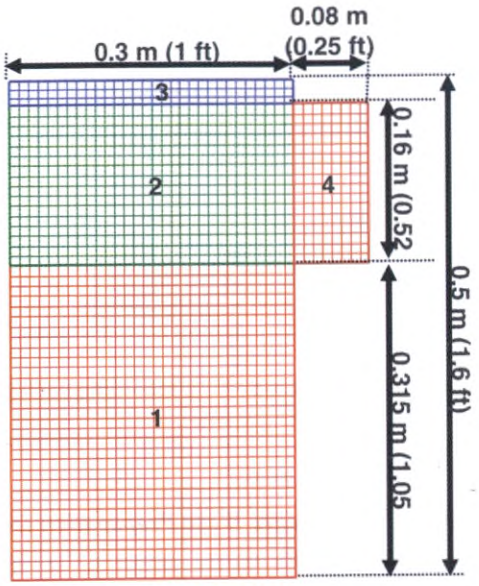

Figure 16 : Geometry and Meshing

4.3.2. Calculation Preparation

Once the global geometry is specified for the calculation, the initial conditions as well as the boundary conditions must be defined.

Figure 17 shows the general overview and the location of the gas bubble at the initial instant of the calculation. Indeed the gas bubble is already created and under pressure (overpressure depending on the arc current). The bubble is centred at (0.15 m ; 0.16 m) or (6 in ; 6.4 in), is surrounded with liquid (oil) and its diameter is 0.1 m (4 in).

All boundaries except the east-border of block 4 are considered walls (5 in Figure 17). The last boundary corresponds to the TP location, split in three sections (35, 335 and 3335 in Figure 17) that behave as walls, as soon as the pressure in their vicinity did not reach the RD calibrated pressure (set at 0.8 bar/11.6 psi). Once the calibrated pressure is reached in the vicinity of the « TP border », each of the sections opens with a delay compared to the previous section opening. The first section will open 3 ms after the overpressure detection (physical time of the RD bulge before the opening), the second one will open 6ms and the last one 9 to 20 ms after the detection. The progressive opening is more in accordance with the experimental reality. Once opened, the border is considered a subsonic inlet/outlet.

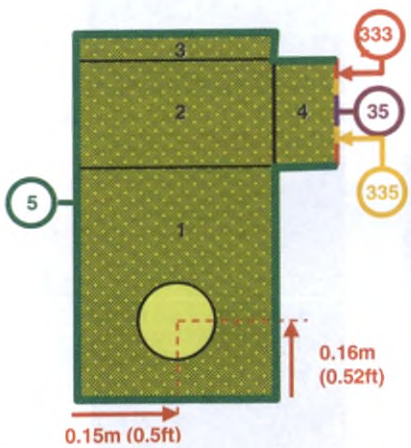

Figure 17 : Initial and Boundary Conditions - EDF

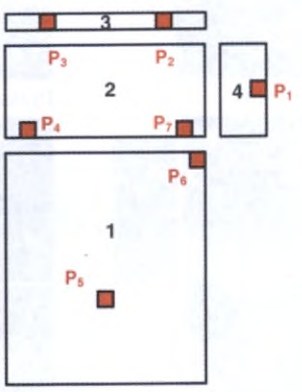

Figure 18 : Virtual Pressure Sensor Locations - EDF

Pressure sensors are located to measure numerical pressure profiles at different places similar to the location of the physical sensors, which enables us to compare numerical and experimental results (Figure 18). Sensors locations are displayed in
Table 5.

Table 5: Sensor Locations

Sensors	Location	
P1	(0.38m ;0.395m)	(15.2in ;15.8in)
P2	(0.2m ;0.5m)	(8in ;20in)
P3	(0.1m ;0.5m)	(4in ;20in)
P4	(0.05m ;0.35m)	(2in ;14in)
P5	(0.15m ;0.13m)	(6in ;5.2in)
P6	(0.3m ;0.23m)	(12in ;9.2in)
P7	(0.25m ;0.35m)	(10in ;14in).

We use the time step $\Delta t = 810^{-7}$ s recording each parameter every $1.6\ 10^{-1}$ ms.

4.3.3. Results

4.3.3.1. Modelled Pressure Wave Propagation Description

The results of this simulation are shown in the Figure 19. In this case and for all studies regarding arcing inside transformer tanks, the pressure is a strong dynamic and spatially non-uniform phenomenon. The initial overpressure generates a symmetrical pressure wave which propagates in an isotropic way and interacts with the structure walls.

This wave spatial dependence is actually noticeable when the reflected waves from the walls interact with each other and focus in sharp parts of the geometry (lower corners at t= t=2.1 10^{-1}ms). At t=5.9 10^{-1}ms and due to a complex interaction, the pressure waves create local overpressures high enough for the pressure to reach the Rupture Disk calibrated burst pressure.

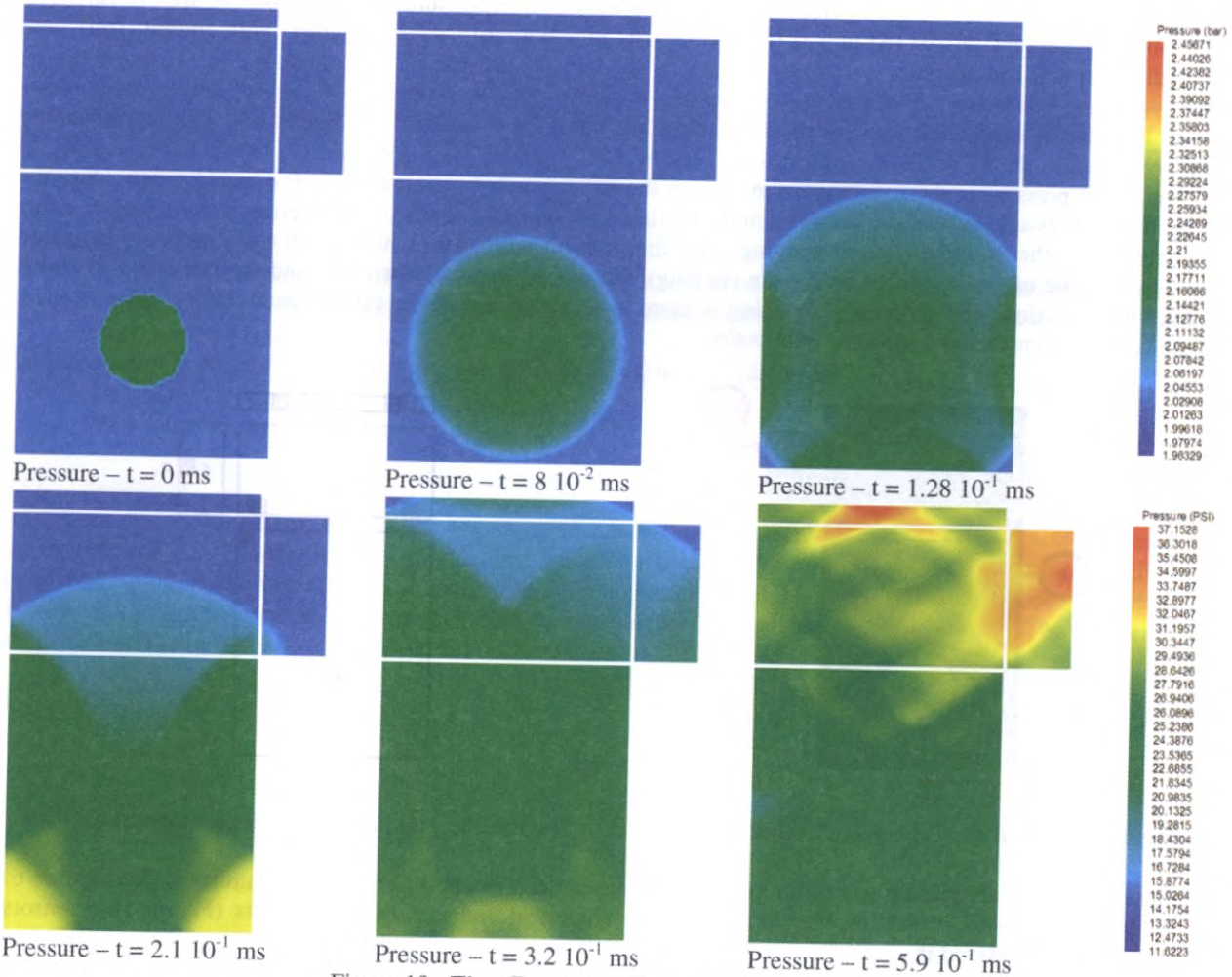

Pressure – t = 0 ms

Pressure – t = 8 10^{-2} ms

Pressure – t = 1.28 10^{-1} ms

Pressure – t = 2.1 10^{-1} ms

Pressure – t = 3.2 10^{-1} ms

Pressure – t = 5.9 10^{-1} ms

Figure 19 : Time Dependent Pressure Map

4.3.3.2. TP Opening Study

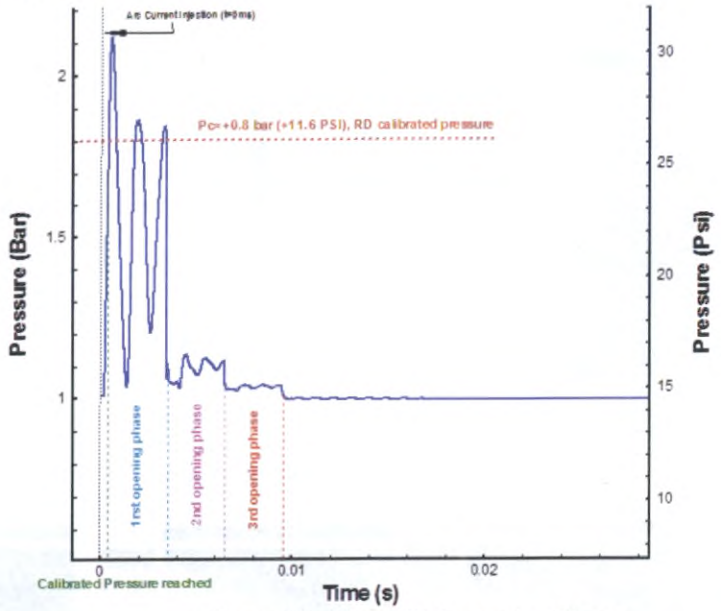

Figure 20 : Three TP Activation Phases

On Figure 20, the TP opening that happens in three phases, results in a huge pressure drop as soon as the TP has begun activating: The first phase is responsible for the most of it while the two others can be distinctly seen but have a smaller influence on the pressure drop.

The Rupture Disk opening due to the inner overpressure results in the oil motion that can be noticed due to the non-zero exit flow-rate at the TP location. The Figure 21 and Figure 22 (83 ms long 5kA arc) prove the correlation between depressurisation and the oil exhaust. The time step during this simulation is $\Delta t = 2\ 10^{-6}$ s for a total physical duration of 160 ms. The data maps (pressure, velocity) were recorded every 4 ms.

The three TP opening phases are shown on the Figure 22 (progressive oil exit flow-rate increase from t=4 ms to t=28 ms). During this opening, the gas bubble is expanding. The flow-rate begins decreasing after t=28 ms. Simultaneously, the pressure evolves: in the first instants the initial overpressure inside the gas bubble propagates and reaches the Rupture Disk whose central area opens 3 ms after the calibrated burst pressure has been reached; at t=4 ms a rarefaction zone appears at the TP location; this depressurisation strengthens between t=4 ms and t=12 ms before the pressure inside the transformer tends to get back to its initial value.

The overpressure is sustained inside the transformer by the energy transfer from the arc to the oil, and disappears as soon as the arc is not fed any longer. At t=96 ms there is no inner tank overpressure. The TP has thus depressurised the transformer tank and prevented the explosion.

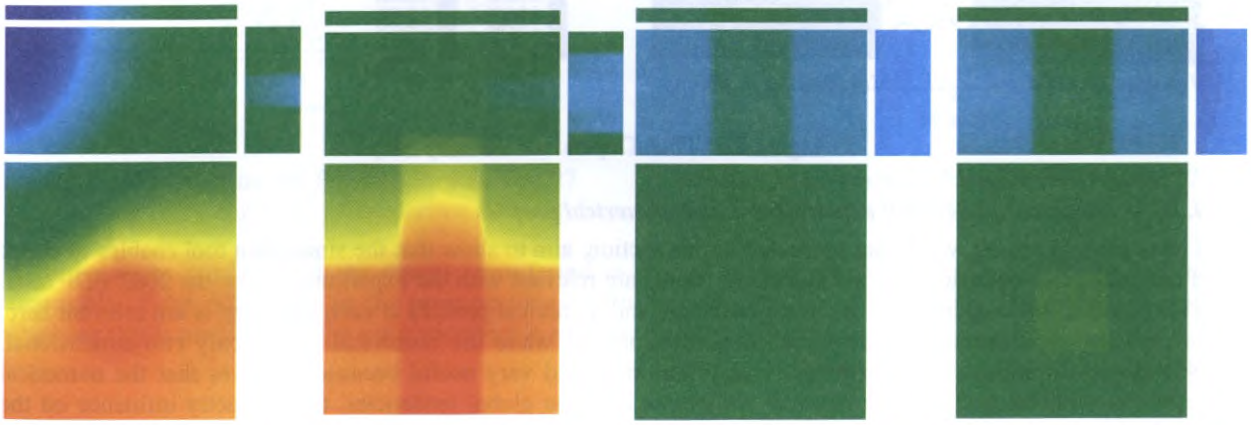

Pressure – t = 4 ms | Pressure – t = 8 ms | Pressure – t = 12 ms | Pressure – t = 28 ms

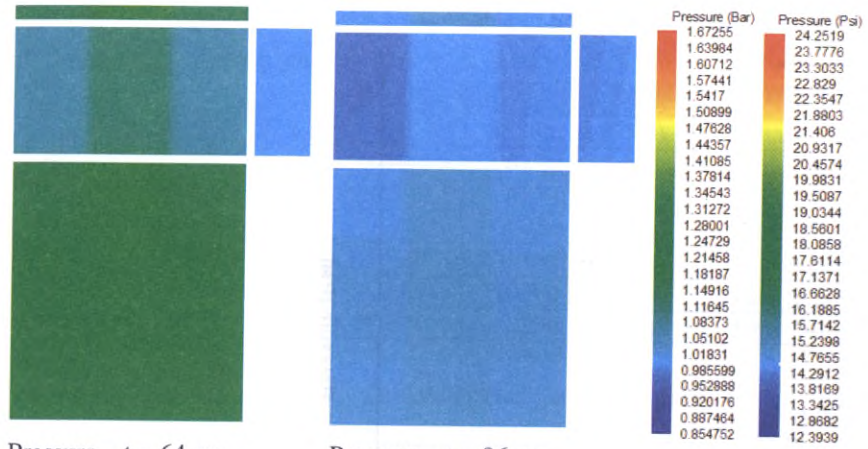

Pressure – t = 64 ms

Pressure – t = 96 ms

Figure 21 : Time Dependent Pressure Maps

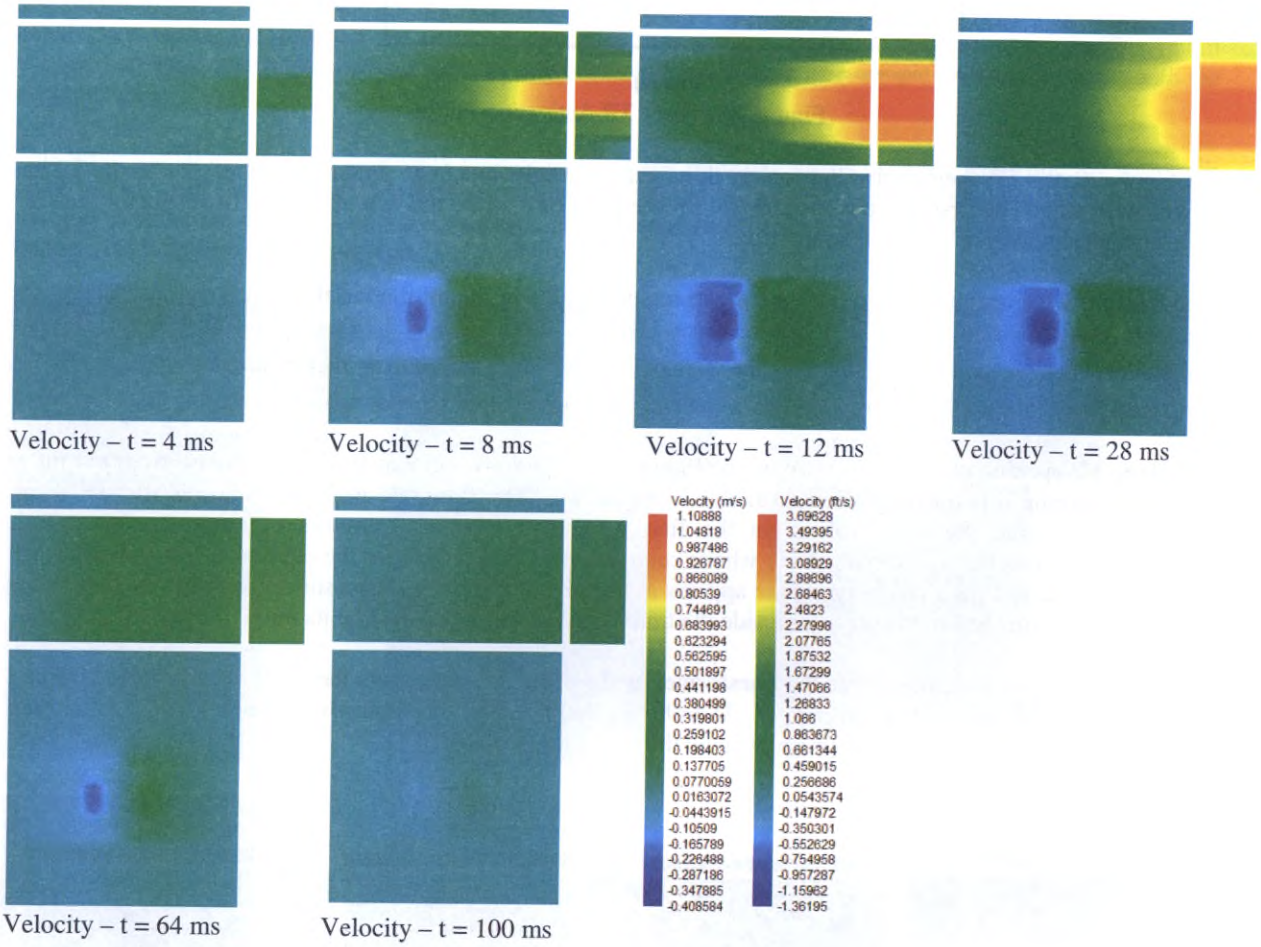

Velocity – t = 4 ms

Velocity – t = 8 ms

Velocity – t = 12 ms

Velocity – t = 28 ms

Velocity – t = 64 ms

Velocity – t = 100 ms

Figure 22 : Time Dependent Velocity Maps

4.3.3.3. Comparison between experimental and numerical profiles

The numerical results, which are presented in this section, aim to show that the simulation tool enables to check if the qualitative behaviours of the numerical results are relevant with the experiments from the 2002 EDF tests. The quantitative comparison between experimental and numerical profiles at each time step is not relevant here. Indeed, the experimental geometry was three-dimensional while the numerical one is only two-dimensional. Nevertheless, qualitative comparisons is very important and very useful because it proves that the numerical results are reliable and that the physical model can describe global tendencies, the geometry influence on the local overpressures, and can prove the TP ability to depressurise the transformer tanks.

Therefore two tests are hereafter displayed. They both rely on the geometry described in Figure 16. The time step used for these simulations is $\Delta t = 210^{-6}$ s with data records every 4 ms. The total physical duration of the simulated phenomenon is 160 ms.

The same nominal 5 kA current feeds the arc in both cases. The maximum arc voltage is set to 2 kV. The arc is fed during 80 ms. The only difference between the two simulations is the energy quantity, transferred to the oil before the TP opens, which has been slightly increased in the very first instants for the first simulation. The qualitative comparison between numerical and experimental pressure profiles is shown on Figure 27.

In both cases, the numerical profiles are in good agreement with the experimental pressure time evolution: the pressure continuously decreases when the energy that is transferred before the TP opens is higher, while the depressurisation is followed by a partial re-pressurisation when the transferred energy is lower.

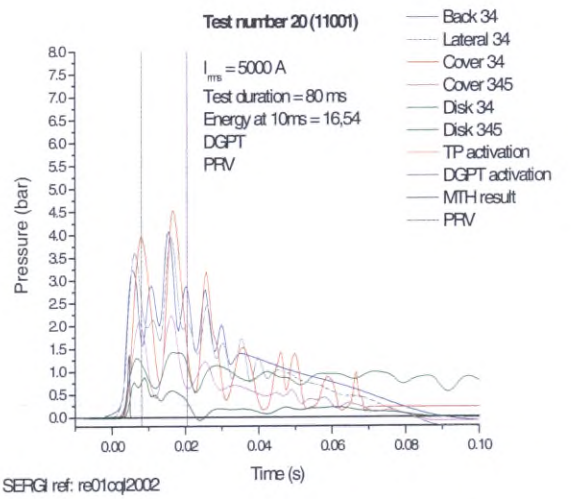

Figure 23 : Experimental Pressure Profile, Test 20

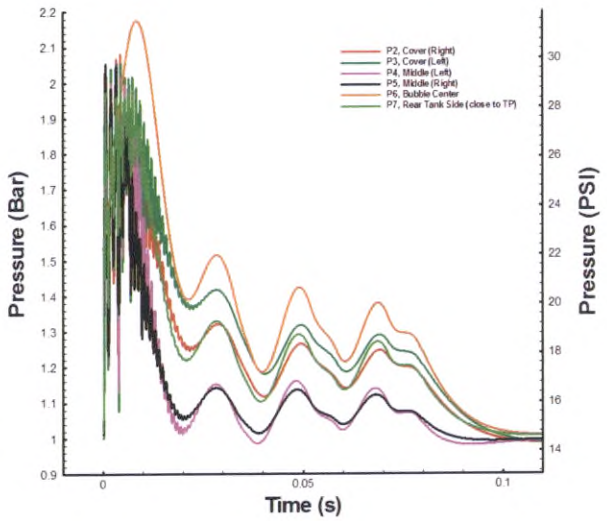

Figure 24 : Numerical Pressure Profile, Test 20

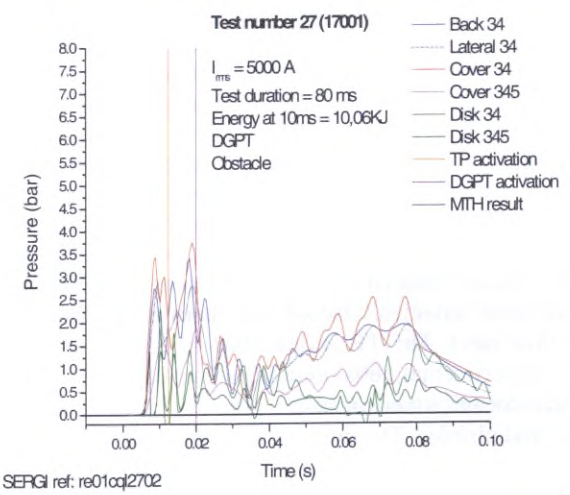

Figure 25 : Experimental Pressure Profile, Test 27

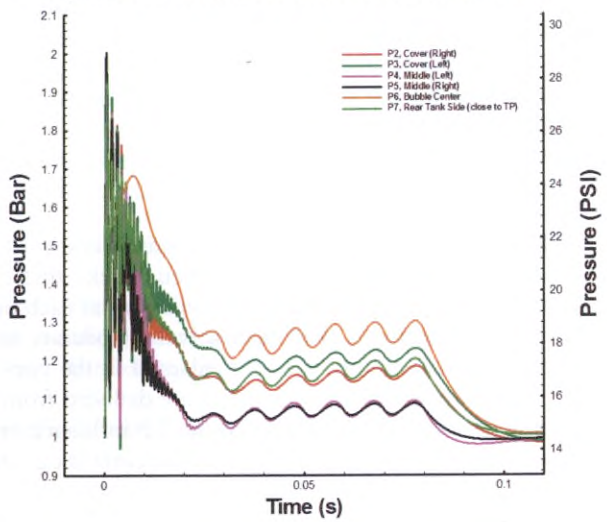

Figure 26 : Numerical Pressure Profile, Test 27

Figure 27 : Comparison Between Experimental and Numerical – EDF Tests

The simulations confirm that the energy, transferred to the oil in the very first instants of the arcing, is responsible of the differences in the pressure time evolution inside the transformer tank. The hydrodynamic behaviour that is predicted by the simulation tool is relevant with the experimental data.

5. Conclusion

SERGI has developed the TRANSFORMER PROTECTOR (TP) in order to prevent the transformer explosion due to an internal low impedance fault. Its efficiency has been experimentally proved by two tests campaigns: the TP always prevented the transformer tank rupture and permanent deformations for the sixty-four tests carried out. Nevertheless, as all physical conditions cannot be experimentally tested, SERGI developed a numerical simulation tool to prove the TP reliability in every kind of situations. The MTH model [16] was built to do so and validated the TP operation on a wide range of severe situations [17][18][19]. SERGI has then upgraded the modelling to be even closer to the physical phenomena during an internal fault by taking into account very transient phenomena such as the pressure waves, their propagation and effects.

In this article the updated model is presented. Gas as well as oil are considered compressible. The full Eulerian model consists of six governing equations which drive the time and space evolutions of the main physical variables that are the gas volume fraction, the mixture density, the gas partial mass, the two components of the fluid velocity, and the mixture total energy, closely linked to the local pressure. The model describes the hydrodynamic, the gravity, the viscous, the heat conduction effects and the arc energy heat transfer.

The hydrodynamic part of the equations is the basis of the modelling and the most important. Indeed, it drives the pressure wave propagation and the wave complex dynamics and interaction with the geometry. It consists of conservation laws (for mixture mass, gas partial mass, momentum, and mixture total energy) and non conservative terms (advection equation for the gas volume fraction). This model has been widely studied in the literature [2][11][14] and was especially designed to describe pressure wave propagation inside liquids. This model fitted our physical requirements and was thus adapted to solve our problems regarding the transformer explosion prevention.

A mathematical analysis showed the theoretical nature and structure of the physical model. The PDE system is hyperbolic and is described by a set of three waves. The structure is thus very similar to the Euler equations'. These equations are widely used in aerodynamics, so that some standard concepts (Riemann problem, waves, PDE analysis) from this field of study were adapted to our field of interest with success.

The other physical effects such as viscosity and thermal are modelled by adapting the concepts from the compressible one-phase flows as well. Gravity effects and arc influence are considered source terms on mixture momentum and total energy equations. The arc energy transfer is modelled by a source term only on the total energy equation whose dynamic value depends on the arc voltage, duration, current, and spatial location, and sustains an internal overpressure as long as the arc is activated. Each phase (gas, oil) follows its own Equation Of State (EOS) for the physical and modelling parameters to be in complete accordance with each other. This is important for the sound speed in each material to be as close as possible to its physical value. The "stiffened Gas" EOS that can accurately describe gases, liquids, and solids has been calibrated to handle oil and its vapour. Moreover, for the model to be physically relevant, an isobaric closure (equilibrium of phase pressures) has been applied, and led to a mixture "Stiffened Gas" EOS that thermodynamically describes the mixture flow.

The numerical method relies on a Finite Volume Method applied onto a two-dimensional geometry which is split into elementary sub-domains called blocks that are discretised by a structured mesh. On each elementary calculation cell, all variables are constant at each time step, but are updated from one step to another. Dedicated numerical methods (Riemann solvers, Godunov space and time schemes, viscous and thermal flux treatment, boundary conditions) are then adapted to the two-phase flow field. The TP is described by specific boundary conditions, whose characteristics are deduced from the TP experimental behaviour. This part is one of the most important because it simulated the TP influence on the transformer inner pressure. The model and simulation tool are thus complete and can handle complex geometries, and physics. The numerical methods are robust.

Their capabilities were illustrated: results from simulations performed with the EDF test geometry are displayed. These simulations show the TP activation and its influence on the depressurisation process. They prove the TP prevents the tank rupture. The two pressure time evolution patterns, highlighted by the results of the EDF tests 20 and 27, are well predicted by the simulation tool: the difference in the pressure patterns seem to strongly depend on the energy transferred by the arc to the oil in the very first arcing instants i.e. on the first pressure peak amplitude.

The purpose of these simulations was only a qualitative comparison and not a complete quantitative validation, which is the subject of the article [21]. Indeed, in [21] a quantitative comparison is carried out using the experimental data collected during the CEPEL test campaign; in that paper TP activation characteristics are studied in details and comparisons between simulations and experiments show a good agreement, so that the numerical tool is validated.

6. References

[1]. R. ABGRALL, "*How to prevent pressure oscillations in multi-component flow calculations: A quasi conservative approach*", Journal of Computational Physics, vol. 125, pp. 150-160, 1996.

[2]. G. ALLAIRE, S. CLERC & S. KOKH, "A *Five Equation Model for the Simulation of Interfaces between Compressible Fluids*, Journal of Computational Physics, vol. 181, 2, pp. 577-616, 2002.

[3]. M.R. BAER & J.W. NUNZIATO, "*A Two-phase Mixture Theory for the Deflagration to Detonation Transition in Reactive Granular Materials*", International Journal of Multiphase Flow, vol. 12, 6, pp. 861-889, 1986.

[4]. G. BRUN, J.M. HERARD, D. JEANDEL & M. UHLMANN, "*An Approximate Roe-type Riemann Solver for a Class of Realizable Second Order Closures*", International Journal of Fluid Dynamics, vol. 13, 3, pp. 223-249, 2000.

[5]. F. DUBOIS, "*Boundary conditions and the Osher scheme for the Euler equations of gas dynamics*", internal report CMAP 170, Ecole Polytechnique, Palaiseau, France, 1987.

[6]. A. FORESTIER, J. M. HERARD & X. LOUIS, "*A Godunov-type solver to compute turbulent compressible flows*", CRAS, I-324, pp. 919-926, Paris, France, 1997.

[7]. E. GODLEWSKI & PA. RAVIART, "*Numerical Approximation of Hyperbolic Systems of Conservation Laws*", Press, Applied Mathematical Sciences, vol. 118, ed. Springer Verlag, Berlin, 1996.

[8]. S.K. GODUNOV, "*A Finite Difference Method for Numerical Computation of Discontinuous Solutions of the Equations of Fluid Dynamics*", Math Sb., vol. 47, pp. 357-393, 1959.

[9]. A.K. KAPILA, R. MENIKOFF & D.S. STEWART, "*Two-phase Modelling of Deflagration to Detonation Transition in Granular Materials: Reduced Equations*", Physics of Fluids, vol. 113, 10, pp. 3002-3024, 2001.

[10]. O. LE METAYER, "*Modélisation et résolution de la propagation de fronts perméables – Application aux fronts d'évaporation et de detonation*", Ph. D. Thesis, Université de Provence, Mechanics & Energy, Marseille, France, 2003.

[11]. J. MASSONI, R. SAUREL, B. NKONGA & R. ABGRALL, "*Proposition de méthodes et de modèles eulériens pour les problèmes à interfaces entre fluides compressibles en présence de transfert de chaleur*"/ "*Eulerian model and method proposal for flows with interfaces in presence of heat transfers*", International Journal Of Heat and Mass Transfers, vol. 45, 6, pp. 1287-1302, 2002.

[12]. A. MURRONE & H. GUILLARD, "*A Five Equation Reduced Model for Compressible Two-phase Flow Problems*", Journal of Computational Physics, vol. 202, Issue 2, 2005.

[13]. R. SAUREL & R. ABGRALL, "*A multi-phase Godunov Method for Compressible Multi-fluid and Multi-phase flows*", Journal Of Computational Physics, vol. 150, pp. 425-467, 1999

[14]. R. SAUREL & R. ABGRALL, "*A Simple Method for Compressible Multi-fluid Flows*", SIAM J. of Scien. Comput., vol. 21, 3, pp. 1115-1145, 1999.

[15]. R. SAUREL & O. LEMETAYER, "*A Multi-phase Model for Compressible Flows with Interfaces, shocks, detonation waves and cavitation*", Journal Of Fluid Mechanics, vol. 431, pp. 239-271, 2000

[16]. SERGI, "*Development of a Magneto-Thermo Hydrodynamic Model and Design of a Transformer, On load Tap Changer and Bushing Oil Cable Box, Explosion and Fire Prevention*", IEEE Publication, ref. rpiip01a, 1999.

[17]. SERGI, "*Comparison of the SERGI developed Magneto-Thermo Hydrodynamic Model results with measurements made on a 160KVA Transformer*", IEEE Publication, ref. rpijp01a, 2000.

[18]. SERGI, "*Study and Design of Power Plant Transformers Explosion and Fire Prevention*", Australia, TechCon 2001, ref. rpitp05a, 2001.

[19]. SERGI, "*Transformer Relief Valves efficiency calculations by comparison to the SERGI TRANSFORMER PROTECTOR during short-circuits*", ref. rpisp01a.

[20]. SERGI, "*Transformer Explosion and Fire, Guideline for Damage Cost Evaluation, TRANSFORMER PROTECTOR Financial Benefit*", ref. fTPoa03a, 2004.

[21]. SERGI, "*TRANSFORMER PROTECTOR Live Tests on Large Transformers: Analysis and Simulations*", Sydney, Australia, TechCon 2006, ref. Arpivp03a, 2006.

[22]. N. THEVAND, "*Contribution à l'Etude Numérique des Ecoulements Instationnaires et Visqueux de Mélanges Gaz-Particules Dilués*", Ph. D. Thesis, Université de Provence, Méchanics & Energy, Marseille, France, 1999.

[23]. E. TORO, "*Riemann Solvers and Numerical Methods for Fluid Dynamics*", Press, ed. Springer Verlag, Berlin, 1997.

7. Biography

Dr. Guillaume PERIGAUD
Research Department Manager, SERGI-Holding
Diploma of Mechanical Engineering, and MSc in Transfers and Fluid Mechanics, ECN, Nantes, France (2000).
Doctor in Mechanics and Energetics, Université de Marseille I, France (2003).

Eng. Héloïse CUNY
Research Engineer, SERGI-Holding
Diploma of Mechanical Engineering, and MSc in Dynamics and Complex Fluids, ENSAM, Paris, France (2004).

Eng. Sylvain Prigent
Development Department Manager, SERGI-Holding.
Saint-Louis Polytechnic Institute, EPMI, Paris, France (1999).

Dr. Philippe MAGNIER
SERGI Holding Chairman
M.B.A., CPA, Paris (1988).
Doctor in Nuclear Physics, Université Paris Orsay (1974).

TRANSFORMER EXPLOSION AND FIRE PREVENTION
Live Tests on Large Transformers: Analysis and Simulations

Guillaume PERIGAUD (Research Department Manager)
Héloïse CUNY (Research Department Engineer)
Sylvain PRIGENT (Development Department Manager)
Philippe MAGNIER (CEO)
SERGI Holding, 186 av. du Général de GAULLE, 78260 ACHERES, FRANCE

Abstract

An essential step for SERGI is to show the TRANSFORMER PROTECTOR (TP) efficacy for all transformers and all types of rupture of insulation. Its research program philosophy is thus to maintain a strong connection between experiments and the theoretical developments.

Up to now, two TP test campaigns have been performed, both under the worst conditions by creating low impedance faults leading to electrical arcs inside the transformer tank dielectric oil. In 2002, Electricité de France performed 28 TP tests. Then, in 2004, a second campaign of 34 TP tests was carried out by CEPEL, the Brazilian independent High Voltage Laboratory. For the 62 tests, each transformer was equipped with the TP, which reacts directly to the moving dynamic pressure peak, shock wave, caused by the low impedance fault.

During the two TP test campaigns the phenomena discovered with the SERGI Magneto-Thermo-Hydrodynamic Model (MTH) were confirmed and the results are presented in this article.

The gas volume generated during an electrical arc is a logarithmic function of the arc energy. The gas production is huge at the creation of the electrical arc because of the intense heat exchange between the arc and the dielectric oil. As soon as gas is produced, the arc is partially or completely surrounded by gas. As a result, the arc energy is used to heat up the gas, to crack the oil vapour into smaller molecules and to change the gas into a plasma. Less and less energy is thus transferred to the oil for it to evaporate. Consequently, the first Mega Joule transmitted to the dielectric oil generates *2.3 m^3 (81.2 ft^3)* of explosive gas, while for a *100 MJ* electrical arc the other *99 MJ* contribute only to *2.0 m^3 (71.1 ft^3)*.

The highest transformer tank acceleration is reached at the time of the creation of the electrical arc, when liquid is suddenly and intensely vaporised. During these tests, for a transformer weight of 72 tons the acceleration reached more than *400 g (g=9.81 m/s^2 i.e. 32.2 ft/s^2)* showing that the applied faults are rather considerable.

When an electrical arc occurs, only one pressure peak is generated. The initial energy transfer is almost instantaneous, and so is the phase change. Because of the oil inertia, the gas is very quickly pressurised. As it is more difficult to vaporise a liquid than to crack oil-vapour into smaller molecules, the arc location would mainly remain in the gaseous phase after and less gas will be produced. As a result, when comparing tests for which pressure peaks are respectively equal to *8 bar (116 psi)* and *8.8 bar (127 psi)*, the corresponding arc energies vary by an order 10 of magnitude (*0.1 MJ* and *1 MJ* respectively).

The correlation of the results obtained between arc energy and dynamic pressure demonstrates that the arc energy is not the key parameter during transformer tank explosion, which is in opposition with the common electrical engineers belief.

One of the purposes of the CEPEL tests was to demonstrate the tank's ability to withstand the dynamic pressure wave before the TP depressurises the tank. The tank's ability to withstand the dynamic pressure has thus been tested for pressure peaks up to 10 times over the static pressure limit and 4 times longer than inside the largest existing transformer. To achieve this result air was added to oil, as 1% of air inside the dielectric oil reduces the shock wave speed by a factor of 10, from *1200m/s (4000ft/s)* to *128m/s (426ft/s)*. During the tests, the highest TP activation time was 57 milliseconds for a shock wave travelling distance of 4 meters *(m)*. With normal, non-polluted oil, the TP activation time would be 6 milliseconds. In this case, the tank has withstood the dynamic pressure 10 times longer than with non-polluted oil. As an illustration, with normal oil, 57 milliseconds

correspond to a shock wave travelling distance of *68 m (220 ft)*. Such a transformer does not exist as it would be 4.5 times larger than the *750 MVA* transformer used here in the article for simulations.

The ability of the TRANSFORMER PROTECTOR to prevent the tank explosion during low impedance faults has been demonstrated. Due to the TP very low inertia to operate compared to the time for the tank to rupture, the overpressure in the transformer tank returns to the static pressure calibration level in 3 milliseconds after the TP has activated. This confirms the calculated value of 3.5 milliseconds obtained with the MTH Model and published by SERGI in 2001 [18].

During the 62 tests, the TP always prevented transformer explosion and any kind of damages or permanent tank deformation.

The other CEPEL tests' main purpose was to compare the experimental results to the simulations carried out due to an extensive software integrating the pressure wave propagation and the TP influence. For these simulations, a compressible two-phase flow model was adapted to upgrade the SERGI MTH Model.

Various physical effects (compressibility, viscosity, gravity, arc influence, and heat transfers) are taken into account. Numerical tests regarding the biggest transformer used for the CEPEL tests are shown for comparison to experiments. The strong interaction between theory and experiments leads to the validation of the numerical tool as well as the physical modelling and empirical laws. Using simultaneously numerical simulations and experimental data, several results are clarified regarding gas volume generated by an electrical arc, the geometry influence, the pressure peaks and pressure wave propagation.

The depressurisation of large transformer tanks is thus numerically studied when considering extrapolated electrical fault conditions. For the shock wave propagation, the worst case is the maximum distance possible between the fault location and the TP. The biggest transformer chosen for the CEPEL Tests had a maximum distance possible between an electrical arc and the TP of *8.5 m (28 ft)* which corresponds nearly to the half of the maximum distance for a *750 MVA* transformer, *15 m (49 ft)*. The results show the TP efficacy even for these severe conditions with only one Depressurisation Set.

TRANSFORMER EXPLOSION AND FIRE PREVENTION
Live Tests on Large Transformers: Analysis and Simulations

Guillaume PERIGAUD (Research Department Manager)
Héloïse CUNY (Research Department Engineer)
Sylvain PRIGENT (Development Department Manager)
Philippe MAGNIER (CEO)
SERGI Holding, 186 av. du Général de GAULLE, 78260 ACHERES, FRANCE

1. Introduction

Transformer explosions are caused by low impedance faults that result in arcing once the oil loses its dielectric properties. Oil is then vaporised, and the generated gas is pressurised because the liquid inertia prevents its expansion. The pressure gap between the generated gas bubbles and the surrounding liquid oil generates pressure waves, which propagate and interact with the tank structure. They cause the pressure rise that leads to the tank explosion. These explosions result most of the time in very expensive damages for electricity facilities [20]. Realising that the transformer explosion prevention is the sole effective solution to avoid such financial losses, SERGI designed and patented worldwide the TRANSFORMER PROTECTOR (TP) in 1999.

The TRANSFORMER PROTECTOR (TP) is a transformer explosion and fire prevention technology based on the direct mechanical response of a Depressurisation Set to the tank inner dynamic pressure increase due to a fault. Since transformers always rupture at their weakest point, the Depressurisation Set is designed to be this weakest point in term of inertia to break before the tank explodes. For that purpose, the Decompression Chamber is equipped with a Rupture Disk (RD). Indeed, after an electrical fault has occurred, the pressure rises, and the Depressurisation Set (DS) opens as soon as the pressure close to the TP has reached the calibrated pressure. Oil is then quickly expelled from the transformer tank, through the Decompression Chamber (DC), and into an Oil Gas Separation Tank (OGST), so that the TP depressurises the transformer tank within milliseconds, and prevents the transformer from exploding. Indeed, once the TP has activated, the mechanical energy is evacuated and the transformer is protected even if the electrical arc is still fed for one second [18],

To design the TRANSFORMER PROTECTOR and to prove its reliability, SERGI has undertaken an extensive research program since 1995:

- In 1998, the "Magneto-Thermo-Hydrodynamic" model, MTH, was finalised [16]. This software was elaborated to simulate the physical phenomena inside a transformer tank during a low or a high impedance fault.
- In 1999, the TRANSFORMER PROTECTOR was designed using the MTH model simulations, and patented.
- By mid- 2000, the first TRANSFORMER PROTECTOR was sold.

Due to the MTH simulations, important issues were studied. The pressure gradients, to which the transformer tank is subjected, were evaluated in [17],[18], and [19]; the time responses of the different protection devices (circuit-breaker, Pressure Relief Valve (PRV)) were compared with TP operation in [19]; the results proved that the TP was the only efficient way to prevent the transformer explosion. In [18], the study of the TP depressurisation and operating times proved the TP efficacy for very high fault levels in large transformers.

In 2002, experiments at Electricité de France High Voltage Laboratory, Les Renardières, on arcing inside oil-filled transformers were carried out to prove the TP efficiency, and to validate the numerical model MTH. The tank explosion was prevented for each of the 28 tests. The pressure gradients, the velocity of the ejected oil, and the gas bubble creation were studied. The experimental results validated the MTH model. However, three important parameters were not measured during this test phase:

- The volume of gas generated during a fault;
- The shock and pressure wave propagation, because of the small transformer size;
- The transformer tank withstand to dynamic pressure.

In 2004, at CEPEL (Centro de Pesquisas de Energia Eletrica), the Brazilian independent High Voltage Laboratory, experiments on large transformers were carried out to study the gas generation, the pressure wave propagation, the tank withstand to dynamic pressure, and to prove the TP efficiency on large industrial transformers. Many electrical and mechanical experimental data were recorded. The test conditions were severe for the TP and the tank regarding the arc locations, arc currents, and the oil acoustic properties drifting due to the non-replacement of the oil after each test. Air was mixed on purpose with oil in order to slow down the pressure waves, maximising the structure tank excitation duration in order to evaluate the tank withstand limit. Meanwhile, the MTH model had been upgraded to describe the complex dynamics, and to calculate the pressure gradients as well as the pressure wave interaction. The physical model and the associated solving numerical methods are detailed in [21]. Since then both the experiment analysis and the simulation tool have been developed, the former validating the latter, the latter helping carrying the former out. The finite propagation speed of the pressure waves is exhibited experimentally. We demonstrate that the transformer power itself is not a key parameter. The transformer size is the parameter of utmost importance, much more than the fault level.

The aim of this article is to:

1. Introduce the Shock Wave Propagation numerical model that upgrades the MTH;
2. Compare the numerical method and physical parameters measured during a low impedance fault;
3. Understand the TP operation and tank depressurisation;
4. Demonstrate that the TP depressurises the transformer long before the tank ruptures by comparing the excitation duration of the tests made with aerated oil and results obtain with normal oil.
5. Show that the arc energy is not a key parameter when a fault occurs inside the transformer tank.

For that purpose:

1. The pressure wave propagation principles are detailed as well as the mathematical model and the solving numerical method.
2. The CEPEL tests' configuration is recalled. The main results of the test analysis are addressed; the theoretical and experimental results are compared to validate the numerical tool.
3. The TP efficacy is presented for the cases of extrapolated operations.
4. The test results regarding the pressure wave propagation speed, measured with aerated oil, are compared with tests and simulations made with normal transformer oil.
5. The volume of generated gas and the pressure peaks amplitude versus energy are commented.

2. Physical Phenomena and Simulation Basics

2.1. Physical Phenomena

2.1.1. Low Impedance Faults

Low impedance faults, or arcs, appear inside dielectric oil because the liquid loses its electrical insulation properties. An electrical arc occurs in the tank, vaporizes the surrounding oil, and creates a gas bubble. The growth of this bubble causes a pressure increase near the fault that propagates in the tank, interacts with the structure, and causes the transformer explosion when tank is not protected by the TP.

2.1.2. Pressure Waves

Pressure is a local phenomenon: a point in the medium can be subjected to very high pressure, whereas another point may not. The initial overpressure created by the electrical arc generates a symmetric pressure wave (acoustic wave) that propagates until it reaches a wall and interacts with it. This interaction between waves contributes to the pressure rise inside the transformer tank (Figure 1). It is important to note that the pressure is not uniform in the medium, and that the geometry may have a great influence on the local pressure [21].

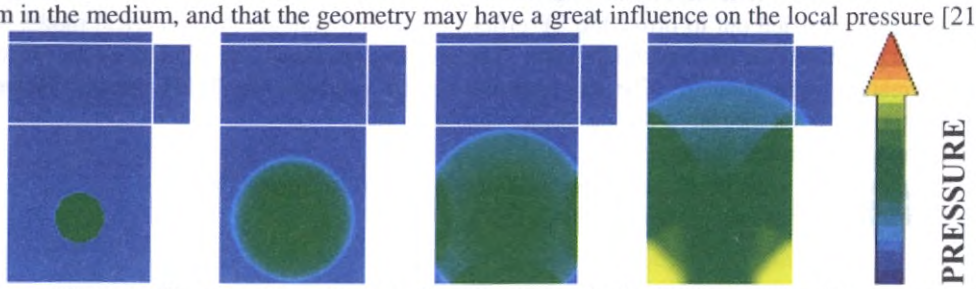

Figure 1 : Pressure Wave Propagation Simulation in the 2002 EDF Test Geometry

In 2004, at CEPEL, TP tests on large transformers were organized to improve the knowledge of transformer explosions, to measure the total gas volume production, to study the pressure wave propagation and test the tank pressure limits compared to the TP efficiency.
To help analysing the experimental results, physical modelling and simulation tools have been developed.

2.2. Mathematical and Physical Modelling

In [21] the physical model and the numerical methods are detailed, but some of the main modelling key points are recalled in the sections hereafter.

2.2.1. Governing Equations

The set of equations used to theoretically and numerically describe the phenomena is an Eulerian model for compressible two-phase flows. The hydrodynamic mathematical model is based on a set of Partial Differential Equations (PDE), which governs the hydrodynamic behaviour of mixtures. One of the major and most interesting model's characteristics is its ability to accurately depict the pressure wave propagation inside liquids and gases. It is detailed in several references [2][12][14] and can be obtained from the general two-phase flow model described in [3][13][15] by an asymptotic analysis [9][12] and an assumption on the volume fraction evolution. Some physical effects are added in the modelling in order to be as closed as possible to reality in term of gravity, viscosity, and heat transfers.

2.2.2. Thermodynamic Closure

For the model to be complete and consistent, a thermodynamic closure has to be added in order to link the mixture pressure to the mixture total energy. Each phase, gas and liquid, is thermodynamically described by its own "Stiffened Gas" Equation Of State (EOS). For each medium, this simple EOS leads to a theoretical sound speed in very good agreement with the experimental one. Then, using the pressure equilibrium assumption, and internal energy additivity property, a "Stiffened Gas" EOS is found for the mixture. This mixture EOS is very useful to handle the artificial mixture zone generated between liquids and gases by the model evolution. More details can be found in the literature [1][2][11][14][15] which show the ability of the method to describe the pressure wave propagation in two-phase flows.

2.3. Numerical Methods

2.3.1. 2D Finite Volume Method and Multi-Block Geometry Description

In order to perform numerical simulations, the physical geometry has to be split into smaller sub-domains called blocks, which are then spatially discretised. These resulting meshes are thus made of small calculation cells where physical variables are assumed to be constant.

A Finite Volume Method is thus adopted to numerically solve the PDE's system. A multi-block strategy is retained and connectivity tables are created in order to make neighbouring blocks exchange information.

2.3.2. Godunov Schemes, Riemann Problems

The model under consideration in the present study is based on a hydrodynamic hyperbolic model for compressible two-phase flows. It is the most important part of the modelling because the pressure waves are depicted by this part of the equations. In a Finite Volume Method, there is a Riemann problem to solve at each cell boundary at each time step in order to compute the numerical fluxes. Details about Riemann problems, their adaptation, and their solving can be found in [6][7][24]. Following the rules detailed in [7] and [24] when presenting the Godunov solver for Euler equations we can also build an exact solver for our model. The various state expressions can be deduced from the ones in [7] and [24]. When dealing with a numerical tool this solver has to be associated with numerical schemes and boundary treatment.

2.3.3. Boundary, Viscous Terms, and Heat Transfer Treatment

The treatment of the boundary conditions can be found in [5]. The viscous and heat transfer terms are accounted for by numerical schemes detailed in [23] and adapted to the two-phase flow model.
The theoretical bases of the simulation tool have been detailed. The simulations helped in understanding and analysing the experimental results from the TP tests on large transformers performed in 2004.

3. Experimental Settings

34 live tests were performed by CEPEL on three standard transformers (**T1, T2, T3**) of significant sizing allowing the shock wave to propagate up to *8.5 meters (28 ft)* between an electrical arc and the TP. These tests were carried out to study the pressure wave propagation and to demonstrate the TP efficiency during a low impedance fault by measuring physical parameters such as pressure, gas temperature, applied current, arc voltage and tank acceleration.

3.1. Experimental Set

Each transformer was equipped with a standard TRANSFORMER PROTECTOR (Figure 2).

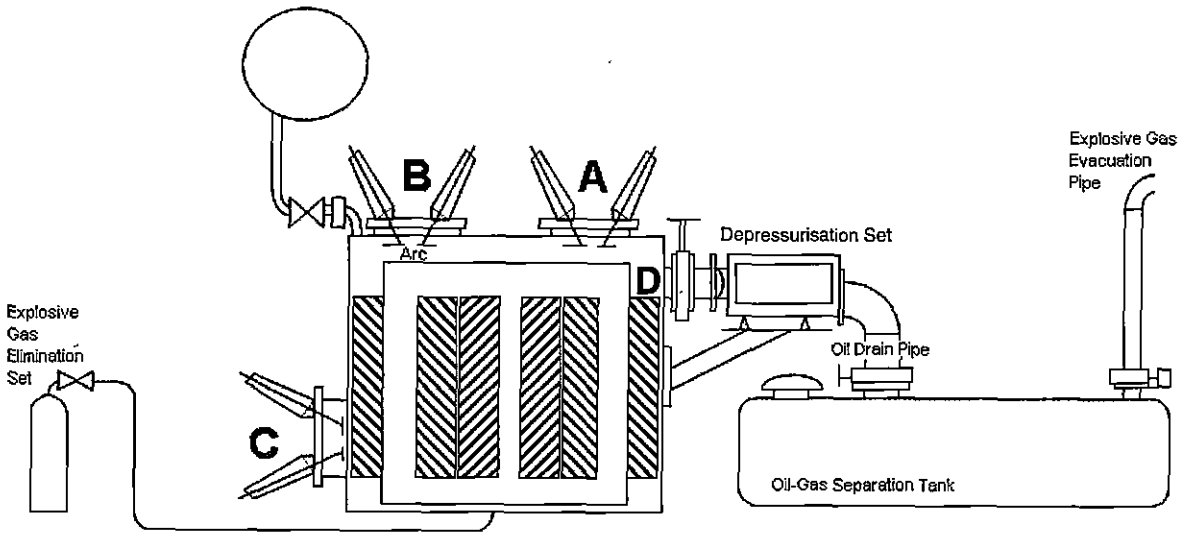

Figure 2 : Life Tests Transformer Principle Drawings

3.2. Arcs

3.2.1. Experiments

To study in detail the pressure wave propagation influence, the arcs were ignited at three different locations, as shown in Figure 2: *on the top cover close to the Decompression Set location* (**position A**), *on the top cover* opposite the Depressurisation Set location (**position B**), and in the lower part of the tank opposite the Depressurisation Set location (**position C**). Position C was the harshest position to test because far from the TP and near the windings, which prevented the pressure waves from easily propagating. Note that the **position D** is shown in Figure 2, and is the location where the TP was installed.

Test characteristics (such as arc locations) are shown in Table 1. The first arc duration, *25 ms*, is the minimum necessary time to create this type of fault; these tests were done by CEPEL for security purposes before the arc current was increased to higher level. Then, most of the tests were carried out with the second, an *83 ms*-fault in order to maximize the generated gas volume and because this time corresponds to the average response time of an old circuit breaker.

Table 1 : Performed tests

Transformer	T3	T2	T1
Current range	*10* to *15 kA*	*5* to *7.5 kA*	*5 kA*
Arc period: *25 ms*	None	2 tests	4 tests
Arc period: *83 ms*	13 tests	8 tests	7 tests
Arc location: A	6 tests	2 tests	3 tests
Arc location: B	5 tests	3 tests	4 tests
Arc location: C	2 tests	5 tests	4 tests

3.2.2. Simulations

The arc influence is of utmost importance in our case. The modelling takes into account the energy transfer from the arc to the oil. This energy transfer is assumed to be 100% efficient so that no energy loss is considered. This transfer results in a local pressure rise governed by the energy source term $\dot{E}$ ($\dot{E} = W \times H_{\chi}(\underline{x}, t)$).

The mathematical function $(\underline{x},t) \rightarrow H_{\chi}(\underline{x},t)$ is the arc test function which is 1 when the space point $\underline{x}$ is part of the set χ and t is lower than the arc duration; otherwise, $H_{\chi}(\underline{x},t)$ is zero. $W = U(t)I(t)$ is the instantaneous electrical arc power, where the arc current $I(t)$ is sinusoidal, and $U(t)$ is the electrical arc voltage, modelled by a square wave signal based on current sign and whose amplitude is U_{max}. The maximum voltage values are randomly disturbed up to 15% to account for the arc random behaviour.

3.3. Measurements

A set of curves is presented in Figure 3 which represents a typical set of results (here for test 11, performed on the transformer T2 with a *7 000 A (rms)* arc located in C and applied for *25 ms*).

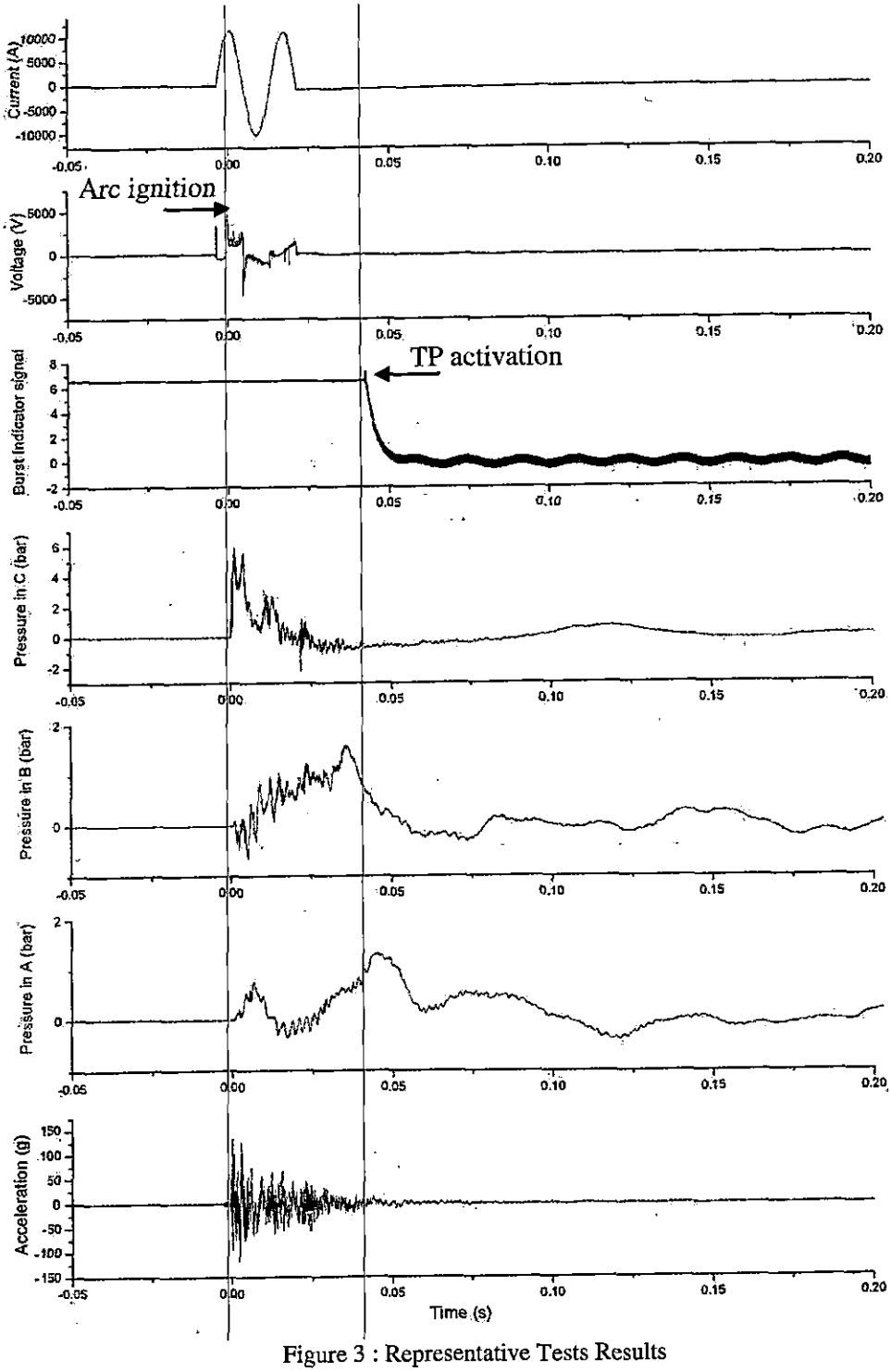

Figure 3 : Representative Tests Results

The analysis of the pressure sensors information helps in understanding the pressure wave phenomena. The arc is generated in position C were the dynamic pressure rises to a peak of *6 bar* (*87 psi*). When the pressure wave propagates the dynamic pressure decreases in C and grows in position B. The pressure peak in position B is approximately *1.8 bar* (*26 psi*), which illustrates the pressure peak decrease during propagation. Then pressure decreases in position B and increases in position A up to *1.4 bar* (*20 psi*), while the shock wave is moving. In the meantime, the pressure wave reaches the TP in position D that depressurises the transformer tank.

4. Analysis and Model Validation

In this section, tests results, their analysis and the comparison with simulations are presented.

4.1. Analysis: Generated Gas

4.1.1. Gas Temperature

When an electrical arcing occurs in a transformer, it vaporizes the surrounding oil and generates explosive gas. The gas temperature measured in the OGST remains constant during each test, and never exceed *60°C* (*140°F*), far from the lowest gas self-ignition level, acetylene (*305°C, 581°F*). The gas temperature at the piping exhaust was always approximately equal to the piping temperature. Therefore, during the 34 tests no flames were detected at the outlet of the Explosive Gas Evacuation Pipe.

4.1.2. Gas Volume: Empirical Law and Comparison with Other Correlations

During the CEPEL test campaign, the electrical arc produced from *1* to *2.3* m^3 (*35* to *88* ft^3) of gas. This volume is plotted as a function of the arc energy in Figure 4. The global trend (dotted curve) is drawn by the following equation:

$$V = 0.44 \ln(E + 5474.3) - 3.8$$

where E is the arc energy and V the generated volume. We compare this trend with the tendencies given in other publications (Table 2).

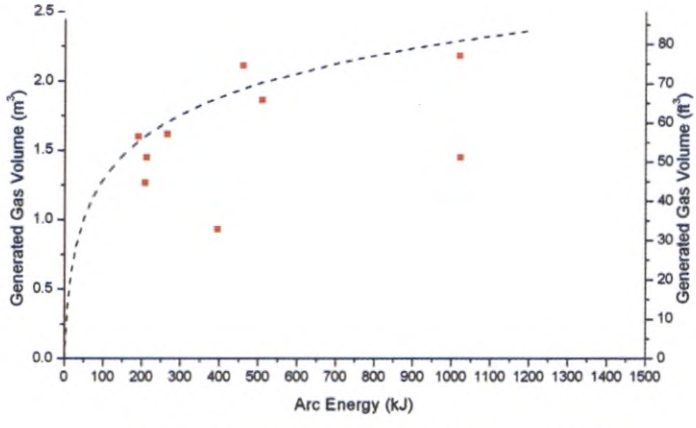

Figure 4 : Generated gas volume v. arc energy

A logarithmic curve seems in accordance with the vaporisation process. Indeed, the vaporisation is very fast and stabilizes once the arc is surrounded with gas (the vaporisation becomes more difficult). When it occurs, the arc is in direct contact with the liquid oil whose thermal conductivity is higher than the vapour's. The oil vaporisation is thus almost instantaneous (Figure 5) because of the huge heat exchange between the arc and the liquid. Then the arc is completely or partly surrounded by oil vapour. In that case the arc energy is used to heat up the gas (thermal agitation), to crack the oil vapour into smaller molecules, and to change the gas into a plasma. Less and less energy is thus transferred to the dielectric oil for it to evaporate (Figure 6). In such a case, the liquid vaporisation is mainly based on the heat exchange at the interface between liquid and gas, so that the gas generation process becomes more and more difficult, which explains the global trend of Figure 4 for the high energy levels.

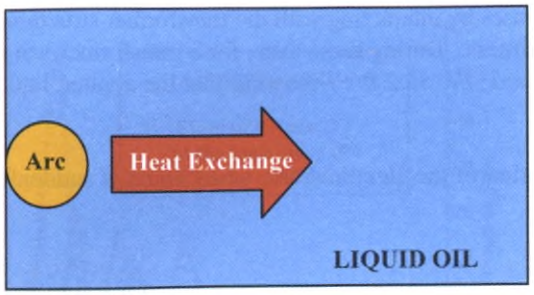

Figure 5: Direct Contact Arc/Liquid Oil – Fast Vaporisation

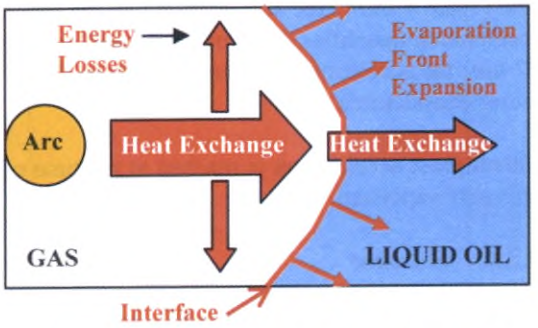

Figure 6: No Direct Contact Arc/Liquid Oil – Slower Vaporisation

A linear extrapolation as shown in Table 2 below is not reliable. In addition, slopes of linear extrapolations vary significantly from one study to another (from $50cm^3kJ^{-1}$ to $500cm^3kJ^{-1}$ ($3\ in^3kJ^{-1}$ to $30.5\ in^3kJ^{-1}$)). By contrast, SERGI model for gas generation:

- Correlates well with the experimental data and is thus more reliable than linear extrapolations because based on experiments;
- Fits the above-explained gas production saturation phenomenon.

Table 2 : Comparison between different publications for any fault levels

Gas Volume / Fault Energy		1 MJ	20 MJ	100 MJ
SERGI $V = K1\ Ln(E + K2) - K3$	m^3	2.3	3.6	4.3
	ft^3	81.2	127	152
Reference [8] $V = 0.1\ 10^{-3}\ m^3.kJ^{-1}$	m^3	0.1	2	10
	ft^3	3.5	70.6	353
Reference [4] $V = 85\ 10^{-6}\ m^3.kJ^{-1}$	m^3	0.085	1.7	8.5
	ft^3	3	60	300

The gas that is dissolved in the oil did not interfere with the generated gas volume measurements if release from the liquid phase: the amounts of the dissolved gas, corresponding to the calculated experimental pressure waves' speeds, range from $0.0052\ m^3$ ($0.2\ ft^3$) to $0.43\ m^3$ ($1.52\ ft^3$), which is negligible compared to the gas generated volumes (cf. section 4.3.3).

From Table 2, when considering the amount of gas generated by a *100-MJ* arc, it can be emphasised that the first Mega Joule transferred to the dielectric oil generates $2.3\ m^3$ ($81.2\ ft^3$) while the other *99 MJ* contribute only to $2.0\ m^3$ ($71.1\ ft^3$). This is to be linked to the amplitude of the strong first pressure peak of the pressure wave, which can be checked in paragraph 4.2.3, Figure 12, where the maximum pressure peak magnitude reaches *10.5 bar (152psi)* for *0.125 MJ* while only *13 bar (188 psi)* was measured for *2.4 MJ*.

4.2. Analysis: Wave Propagation and Fluid/Structure Interaction

At the beginning of the process, when the arc occurs, the tank is sealed and the vaporisation causes the bubble growth which generates a shock wave in the transformer.

4.2.1. Acceleration

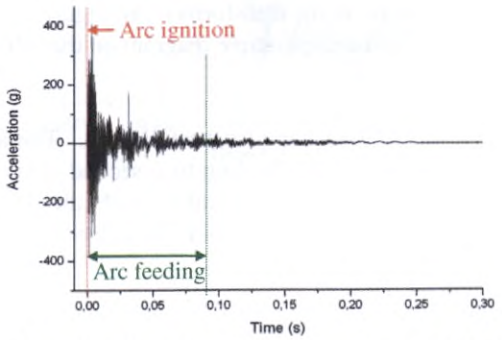

Figure 7: Tank Acceleration Profile - T3, 400g *($g=9.81m/s^2$ i.e. $282\ ft/s^2$)*, Arc Duration=*83ms*

The Figure 7 shows the acceleration that the shock wave causes by interacting with the transformer structure. The acceleration quantifies this tank movement and the fault stiffness. During these tests, for a transformer weight of *72 tons* the acceleration reached more than *400 g (g=9.81 m/s² i.e. 32.2 ft/s²)* showing that the applied faults are rather considerable.

This highest acceleration is reached at the time of the creation of the electrical arc, when liquid is suddenly and intensely vaporised.

4.2.2. Pressure

- **Pressure Profile Evolution at a Single Location**

The pressure in the transformer after an electrical arc has occurred is transient as shown in Figure 8 where an experimental curve is displayed.

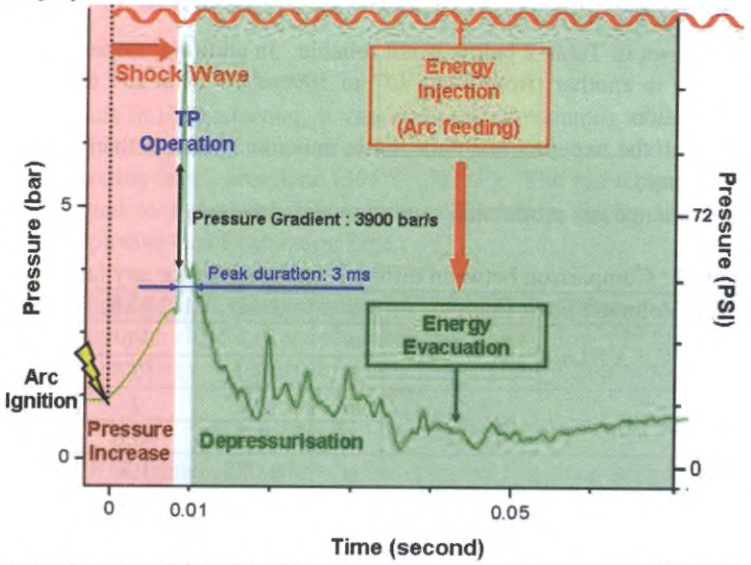

Figure 8 : Pressure Evolution Close to the Arc Location After the Arc Ignition

The different phases are also detailed on this figure: after the arc ignition the pressure locally rises and reaches a maximum level; the waves, generated by the arc, propagate at a finite speed through the transformer and interact with the TP with a pressure gradient of *3900 bar/s (56000 psi/s)*. Three milliseconds after the TP has activated, the pressure is back to the activation level. Some secondary peaks, much lower than the first pressure maximum, can be observed; they are due to wave reflections off the tank walls and reflected waves interactions.

As soon as the TP has activated, it can be noted that the arc can be fed for a period much longer than the standard opening time of a circuit breaker. Even in this severe condition, the pressure would remain at harmless levels for the transformer tanks. This was already emphasized by SERGI in 2001 [18]: in this reference, it was demonstrated that for a *236 kA* short-circuit, an opening of *0.15 m (6 in)* was sufficient to evacuate the energy during a steady feeding of the electrical arc by the inertia of the generator.

- **Local Pressure and Wave Propagation**

The shock wave caused by the electrical arcing propagates in the tank. As predicted by the physical two-phase flow model, the pressure is not homogeneous in the transformer. In Figure 9, experimental pressure profiles are displayed on the right and a simplified associated principle diagram on the left. Each curve shows what happens near each sensor located in positions A, B and C.

The displacement of the shock wave in the tank can also be followed. The arc ignition located in C causes a high-pressure peak. The pressure waves propagate leading to a second delayed lower peak in B, ending in A. For each sensor, the other pressure peaks (smaller than the main peak) are due to wave reflections off the walls. This pressure wave propagation can also be exhibited when studying test-11 chronology in Figure 3.

This proves that pressure is not spatially uniform in the tank, and that the pressure waves propagate at a finite speed, which is in agreement with the physical modelling.

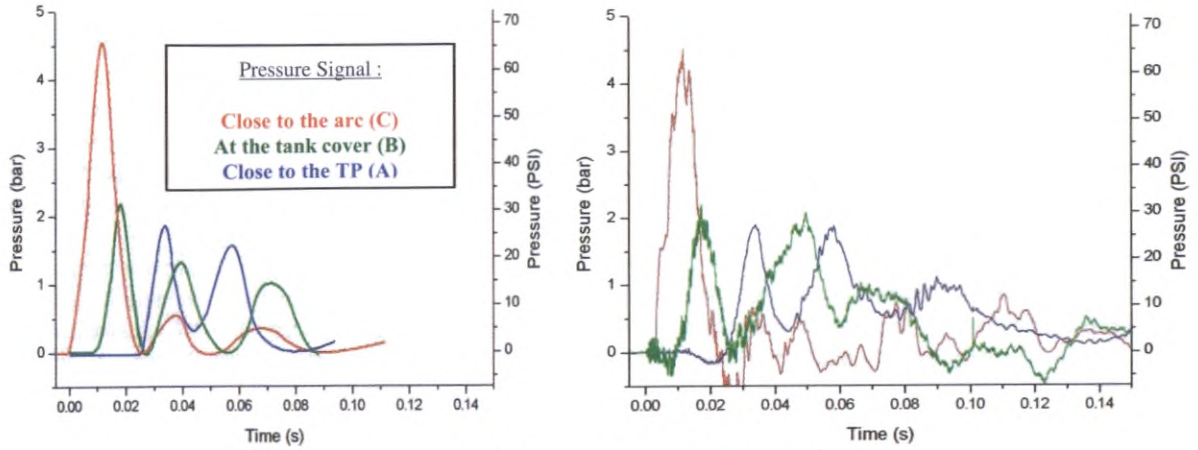

Figure 9 : Pressure measurements model

- **Geometric Signature**

The study of the experimental pressure curves shows that the tank structure has a local influence on the pressure behaviour. Three tests on the same transformer are compared in Figure 10 and Figure 11 (same arc location, but different arc characteristics). The time pressure behaviours during the fault are similar; a characteristic high second peak occurs.

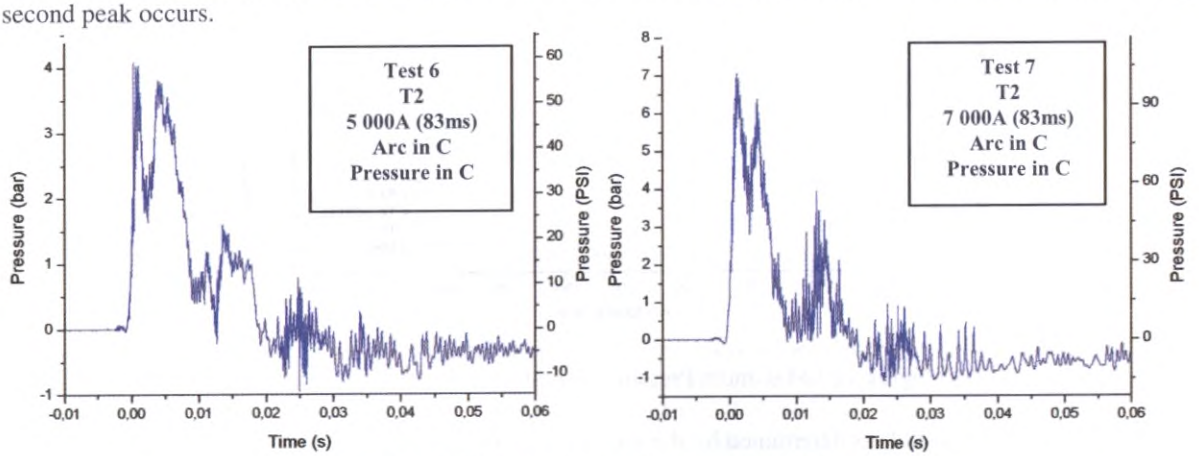

Figure 10, Pressure profiles (tests 6 and 7)

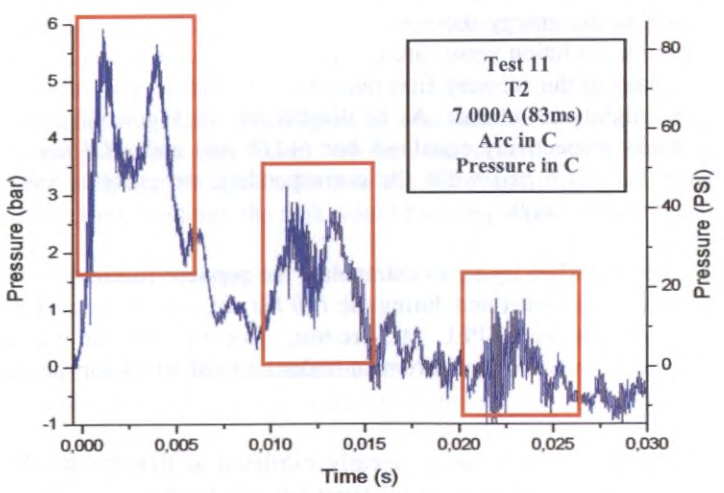

Figure 11 : Pressure profile (test 11)

As explained previously, the waves interact with the structure and reflected waves are generated. These secondary waves have the same pattern (the M-shape located with red rectangles in Figure 11) meaning that the structure has a real influence on the pressure behaviour. The only parameter that seems not to depend on the structure is the level of pressure.

4.2.3. Pressure Peaks and Tank Withstand

- **Pressure Peaks**

Only one main pressure peak has been noticed for each test. The pressure profiles show variations after that main peak but their magnitude remains low compared to the first pressure peak level. Indeed, as the first vaporisation is a non-equilibrium phenomenon, it is more violent than the almost-at-equilibrium vaporisation occurring once the arc is ignited.

Indeed, the initial energy transfer is almost instantaneous, and so is the phase change. The created gas has no time to expand and reach the pressure and temperature equilibrium with the surrounding oil. Because of the oil inertia, the gas gets very quickly under pressure, which generates the first very strong pressure waves.
As it is more difficult to vaporise a liquid than to crack oil vapour, the arc location would mainly remain in the gaseous phase after its ignition. The vaporisation which happens after the gas bubble appearance is smoother and do not really generate physical conditions such as the ones in the very first arc instants. The secondary pressure variations are thus the result of the overlapping waves and structure influence combined with the smooth gas generation influence on pressure.

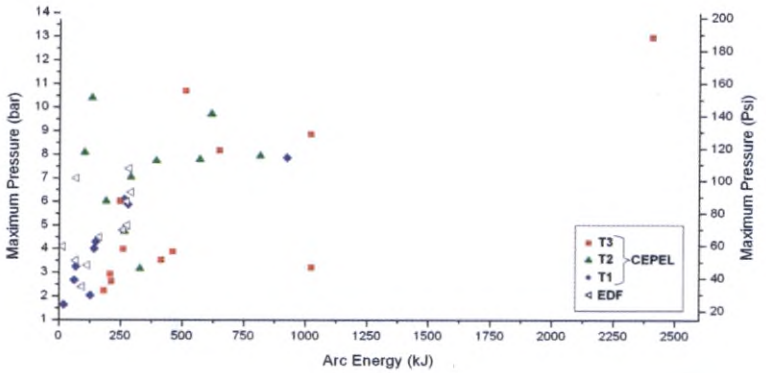

Figure 12 : Maximum Pressure Close to the Arc v. Arc energy

The pressure peaks' amplitude is determined by the created arc. The peaks range from *+1.5* to *+13 bar* (*+21.75* to *+188.55 psi*) for arc energies from *0.01 MJ* to more than *2.4 MJ* as shown in Figure 12. The maximum pressure seems to strongly increase with the arc energy while the energy remains in the low range. This dependence tends to weaken as the energy increases. This behaviour is very similar to the one exhibited in section 4.1.2 for the gas volume evolution versus arc energy. The pressure rise is indeed the result of the strong oil vaporisation that takes place in the arc very first moments. Therefore, gas volume and maximum pressure evolutions versus energy are tightly correlated. As an illustration, the Figure 12 shows that, when comparing tests for which pressure peaks respectively equal *+8 bar* (*+116 psi*) and *+8.8 bar* (*127 psi*), the maximum pressure only varies in *0.8 bar* (*11.6 psi*) while the corresponding arc energies vary within on order 10 of magnitude (*0.1 MJ* and *1 MJ* respectively).

This is a very important statement when trying to extrapolate the pressure maximum values to very high energy arcs. For instance, the amount of gas generated during the *100 MJ* arc, considered in Table 2, is *4.3* m^3, less than twice the gas amount measured for the CEPEL *1MJ*-arc-test. According to the maximum pressure evolution trend versus arc energy, the local pressure would remain under harmful levels for the tank, even in these severe conditions.

Unfortunately no mathematical correlation can be clearly exhibited to link the maximum pressure to the arc energy because of the scattering of the experimental point set and because oil vaporisation kinetic terms are missing to properly carry out an analytical study.

Moreover, Figure 12 shows even if most of the pressure peaks are higher than the commonly admitted transformer withstand static overpressure limit of *+1.2 bar (+17.4 psi)*, there was no tank rupture.

- **Pressure Gradients**

The pressure gradient is the temporal rate of pressure increase. This measurement enables us to quantify the phenomenon strength. The TP is especially useful in protecting the transformer in the high-pressure gradient range (above *25 bar.s^{-1} – 73 psi.s^{-1}*). The pressure gradients have been evaluated close to the arc, so that geometry does not influence their values in large proportions (no damping). Here, the pressure gradients range from *97* to *4 400 bar.s^{-1}* (*1406* to *63 800 psi.s^{-1}*).

The higher the pressure gradients are, the faster the TP operates. Indeed, for 2 tests with the same arc location, the times for the pressure waves to reach the TP are similar, but the time for the pressure close to the TP to reach the calibrated RD burst pressure depends on the pressure gradients close to the TP as shown by the principle diagram displayed in Figure 13.

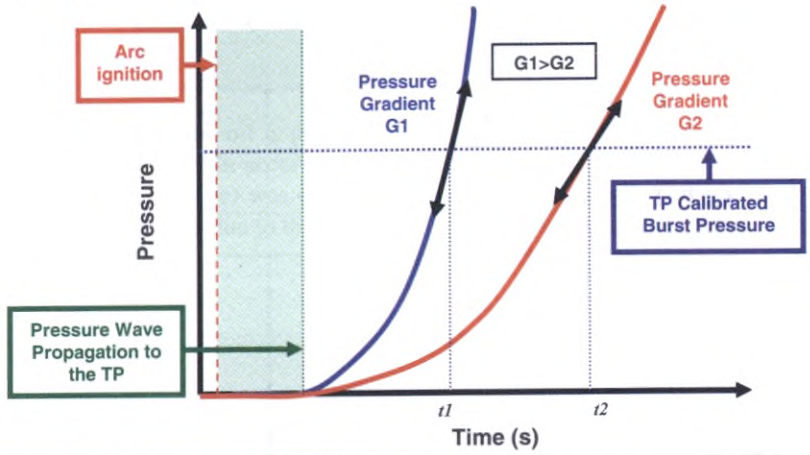

Figure 13 : Influence on TP Activation of Levels of the Pressure Gradient Close to the TP

- **Tank Withstand**

To static pressure: To check the mechanical properties of the transformers, static tests were performed before applying any low impedance fault. The principle was to increasingly apply static pressure to each transformer tank and to measure their withstand limit. The commonly admitted transformer withstand overpressure limit is *+1.2 bar* (*+17.4 psi*). Nevertheless, this limit was only *+0.7 bar* (*+10.15 psi*) for the biggest CEPEL test transformer, T3. Therefore, instead of the +1.2 bar overpressure limit, this new limit (*+0.7bar-+10.15 psi*) has been used in this analysis as a threshold for the tank depressurisation during the dynamic tests. As long as the average static pressure, inside the transformer, remains under this limit, the transformer is safe.

To dynamic pressure: Despite the fact that the local pressure measured during the dynamic tests is on average 6 or 10 times higher than the static withstand limit (Figure 12), no tank damage and no tank permanent deformation occurs because the pressure peaks are very short. In fact, the structure can locally withstand high dynamic pressure increases due to the elasticity of its walls and the TP small inertia to operate. If the pressure had remained above the static overpressure limit, the tank would have exploded.

4.3. TP Influence on the Pressure Evolution

4.3.1. Activation Time

The "activation time" is the addition of the following times:

- The "pressure wave transit time" is the time required from the arc ignition, for the shock waves to propagate and reach the TP;
- The inertia of the TP to operate;
- And the TP burst indicator signal delay.

On average, the TP has activated after about 20 milliseconds (minimum: *4.64ms*, maximum: *45.7 ms*) after the arc was ignited. The maximum distance between the arc location and the TP is the parameter that matters the most for the TP to activate. In the worst situation, the arc occurs in the transformer lower part opposite the Depressurisation Set (location C).

4.3.2. Relation between Transformer Size and Power

This maximum distance is maximised by the sum of the transformer height and length, and is plotted in Figure 14 versus the transformer power. The power of the transformers considered in this statistical study, range from 45 to 750 MVA. The maximum distance for the T3 transformer manufactured in 1969 is about *8.5 m (28 ft)* which in fact corresponds to the size of a 100 MVA transformer manufactured today. The T3 transformer used for the CEPEL tests is thus as large as a recent 100 MVA transformer as shown in Figure 14. The maximum distance between the worst electrical arc location and the TP was *8.5 m (28 ft)* which corresponds to more than the half of the maximum distance for 750 MVA transformer, *15 m (49 ft)*.

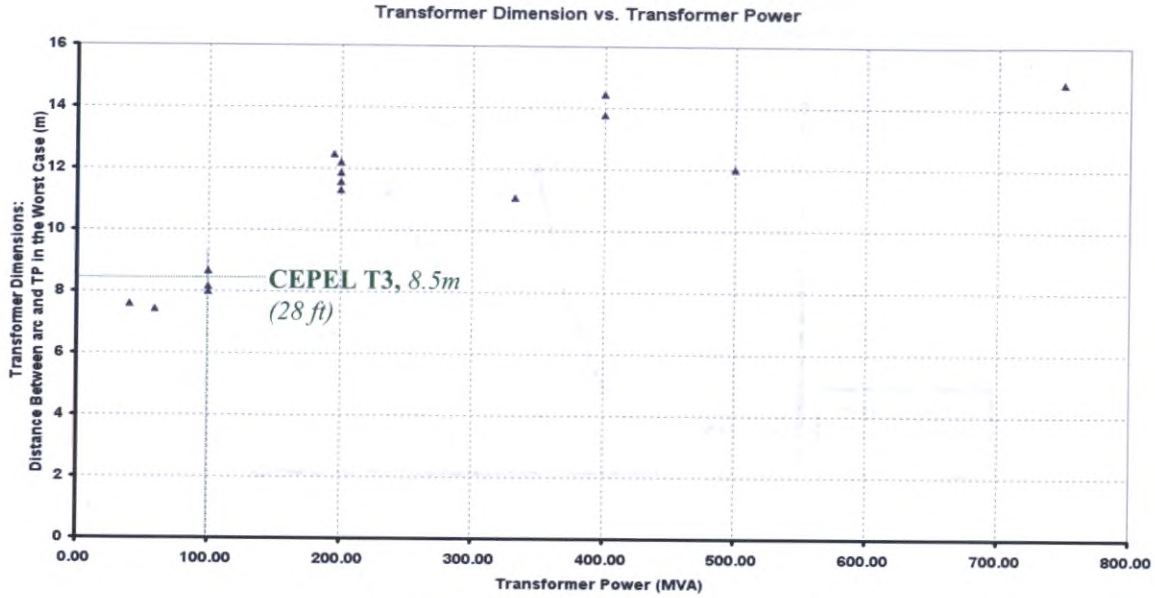

Figure 14 : New Transformer Size versus Power (MVA)

It is thus emphasised that the maximum extrapolation ratio from the tests to non-experimentally-tested simulations is about *2 (15 m/8.5 m)* and not the ratio of the power of the transformers.

4.3.3. Reduction of the Shock Wave Speed by Oil Alteration during the CEPEL Tests

During the CEPEL Tests, the TP activation time was strongly maximised, as the experimental speed of sound was much smaller than the theoretical one. During the tests the oil was polluted on purpose with air to reduce the speed of the shock wave in the dielectric oil. This variation is well described in [25] where the authors deal with mixtures and their acoustic properties. The speeds of sound in an oil and gas mixture, calculated by formula from [25], are stated in Table 3 versus the dissolved gas volume fraction. This table shows the strong influence of the air in slowing the pressure wave propagation. This theoretical fact is in accordance with the calculated experimental speeds of sound.

It can be noticed in Table 3 that *1%* of air inside the oil reduces the speed of a factor 10, from *1200m/s (4000ft/s)* to *128m/s (426ft/s)*. During the tests, *0* to *1%* of air was added. It is obvious that such percentage was very difficult to master so that we could not impose an accurate value for each test. Nevertheless, we can assume that this percentage was on average 0.5% (± 0.5%).

According to the mixture speed of sound formula, stated in [25], for each test, we could evaluate the dissolved gas volumes, corresponding to the experimental pressure wave speeds. They range from *0.043* to *0.0052* m^3 (*0.2* to *1.52* ft^3). It is improbable that the dissolved gas was released in a gaseous phase, so that it would have been accounted in the generated gas measurement. Nevertheless, in case it would have been released , the dissolved gas volume would have been so small compared to the generated gas volume that it would not have interfered with the gas measurements.

Table 3 : Wood/Wallis Mixture Speed of Sound versus Gas Volume Fraction

Gas Volume Fraction	Wallis/Wood Mixture Sound Speed [25]	
	m/s	*ft/s*
0	1200	4000
10^{-6}	1195	3983
10^{-4}	878	2926
10^{-3}	395	1316
10^{-2}	128	426
1	373	1243

In normal transformer operation, the oil is permanently monitored in order to guarantee its physical properties and the speed of the shock waves is in accordance with the theory. Figure 15 shows that the experimental value of the Activation Times (higher curve) was on average about 6 times slower than the theoretical (lower curve). The large scattering of the results is due to the impossibility to master the oil alteration parameters.

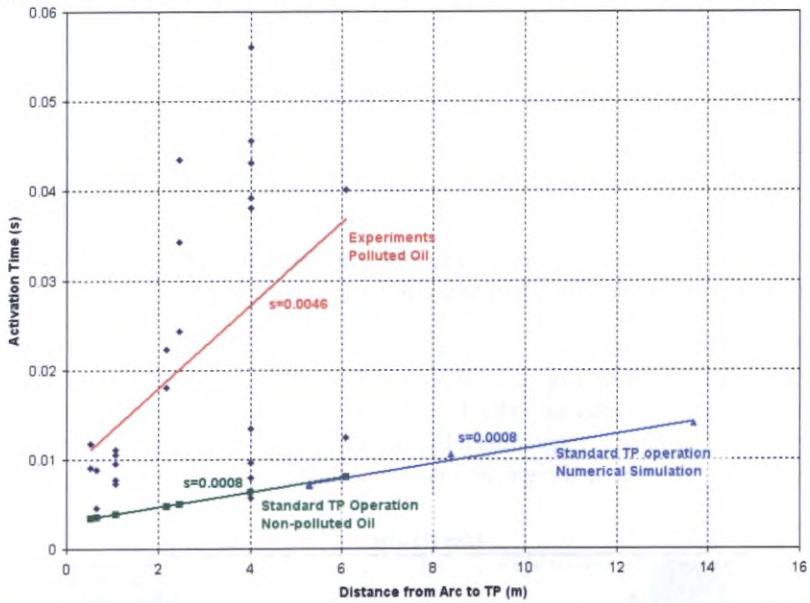

Figure 15 : Theoretical (lower curve) and Experimental (higher curve) Activation Times

On Figure 15 it can be noticed that the highest activation time is *57 milliseconds* for a distance to travel of *4 meters*. With normal, non-polluted transformer-oil, the activation time would be approximately 6 milliseconds. In this case, the tank has withstood the dynamic pressure 10 times longer than with non-polluted oil. With normal transformer oil, *57 milliseconds* correspond to a shock wave maximum distance to travel of *68 meters* (*220 ft*). Such a transformer does not exist as it would be 4.5 times bigger that the *750 MVA* transformer used hereafter in paragraph 5 for simulations.

As a result, it is demonstrated that during the tests the transformers had been subjected to high-pressure levels approximately at an average of 6 times longer than they would have been in case of a normal standard operation. Consequently, we can conclude that in a normal standard transformer operation, the TP will activate 6 times faster, in case of an internal fault. This is another proof that the transformer tank inertia to explode is far greater than the time required by the TRANSFORMER PROTECTOR to depressurise the tank for any transformer size.

It has also to be emphasised that the 3 transformers used by CEPEL have withstood 10 tests each in the worst conditions and that none of them was subjected to explosion or permanent deformations.

4.3.4. Depressurisation Time

The depressurisation time is the time between the TP Opening and when the pressure is definitely under the level of *+0.7 bar (+10.15 psi)*. It is here reminded that the level of *+0.7* bar corresponds to the static pressure limit where leaks appeared on the T3 transformer during the static pressure tests. On average, the TP depressurizes the tank in *116ms*, with a minimum value of *19.7ms*, and a maximum of *347ms*. This experimentally proves the TP ability to depressurise the transformer tanks within milliseconds and prevent the explosion. The previous experimental data and their analysis are very important in the numerical tool validation, which is the subject of the next sections.

4.4. Model Validation

In order to validate the presented mathematical method, whose details are presented in [21] numerical tests are performed and compared to the experimental results. For this comparison, we focus on the most severe tests performed on the T3 transformer, similar to a 100 MVA transformer manufactured nowadays.

4.4.1. Experimental Tests for Comparison

Four experimental tests are shown to compare numerical and experimental results. All characteristics are displayed in Table 4.

Table 4 : Tests retained for comparison between experiments and simulations

Test Number		23	24	31	33
Arc Position		B	C	B	B
Arc Duration	*ms*	83	83	83	83
Maximal Current	*A*	14 476	13 121	34 476	31 783
Maximal Voltage	*V*	979	860	1034	923
Arc Energy	*kJ*	212	208	460	414

4.4.2. Geometry

The outer tank as well as the magnetic core dimensions are detailed in Figure 16. For the simulations, the physical geometry is split into 15 blocks, each of them discretised by a regular Cartesian mesh.

4.4.3. Initial and Boundary Conditions

Boundary conditions are detailed in Figure 16: All boundaries are walls (outer tank as well as internal windings) with which the pressure waves will interact. The TP is numerically modelled and the calibrated burst pressure is set depending on the test simulated. Experimentally, the arc vaporises the oil and creates gas bubbles under pressure. In the initial state we assume the gas bubble has already been created by the arc and the gas is already under pressure.

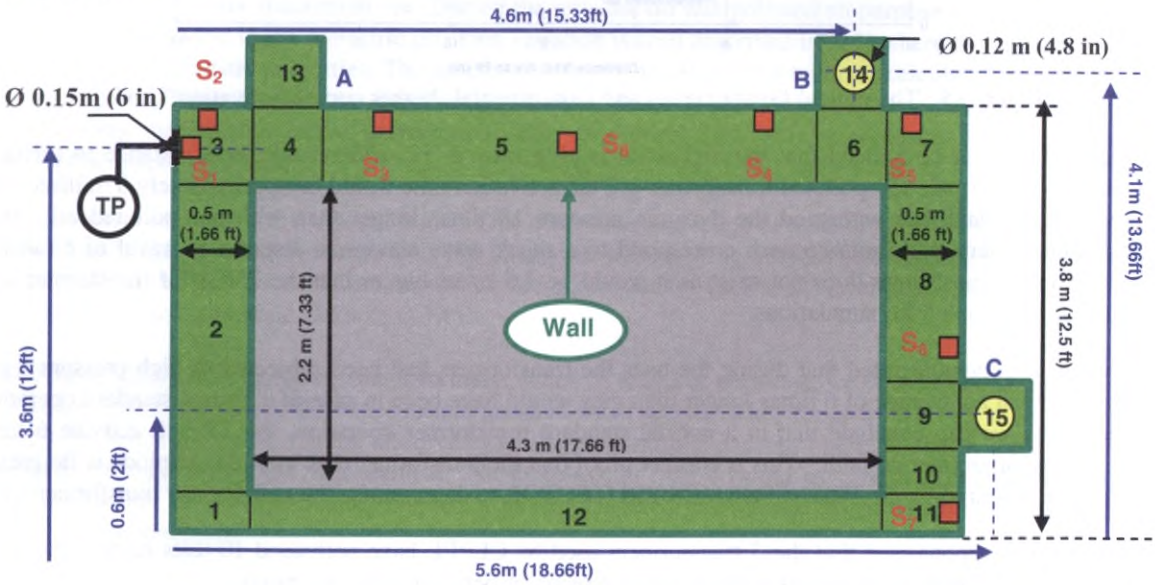

Figure 16 : Boundary and Initial Conditions – T3 Transformer

Thus, the gas bubble generated by the arc is located, in the initial state, either in position B or C, depending on the simulated experimental configuration. Pressure inside the gas bubble and the corresponding density are determined according to the arc energy for each test. The arc characteristics are those of the corresponding experimental test (Table 5).

Table 5 : Initial Conditions and Characteristics for the Simulations

Simulated Tests		23	24	31	33
Arc Location		B	C	B	B
Gas Pressure	*bar*	4.3	2.7	4.3	4.3
	psi	62.4	39.15	62.4	62.4
Gas Density	kg/m^3	4.3	2.7	4.3	4.3
	lb/ft^3	0.27	0.17	0.27	0.27
TP Calibrated Burst Pressure (relative pressure)	*bar*	+1.5	+1.5	+1.5	+0.8
	psi	+21.75	+21.75	+21.75	+11.6
Outer Reference Pressure (absolute pressure)	*bar*	0.1	0.1	0.1	1
	psi	1.45	1.45	1.45	14.5

Moreover, virtual pressure sensors (S_i) are located in the simulation domain in order to compare the experimental pressure profiles to simulated ones (Figure 16). The results of this comparison are shown in Figure 17 and in Figure 18

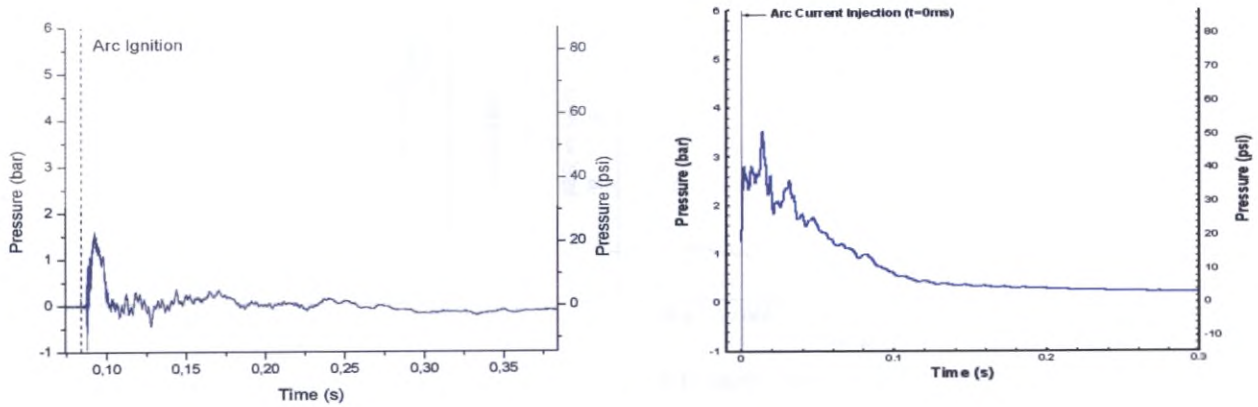

Figure 17 : Test 24 – Pressure profile close to the arc: experiment (left) simulation (right)

4.4.4. Experiment/Simulation Qualitative Comparison

Experimental and numerical results regarding the pressure time evolution are similar. In both cases, the three same phases can be observed: a very sharp pressure rise following the arc ignition, a pressure drop because of the TP activation, and a phase where the pressure alternatively rises and decreases because of the complex wave dynamics due to the wave reflections off the transformer walls (cf.Figure 17 and Figure 18). It can be checked that in both cases the pressure returns to the initial reference pressure.

Besides, we recall that the same time pressure evolution was experimentally noted for tests with the same arc location but different electrical characteristics (cf. Figure 10 and Figure 11). For tests 23, 31, and 33, the arc location is the same.

In Figure 18 where numerical as well as experimental results are displayed, the experimental results are in accordance with the tendency exhibited in the previous sections for tests 6, 7, and 11. The simulated pressure profiles are very similar as well: even if the pressure maxima are not the same in every case, the chronology of the phenomena and the profile shapes are identical.

These similarities between experiments and theory confirm the geometry influence on local pressure profiles.

On each profile, we can notice that the TP influence causes an inner tank average pressure decrease. The pressure oscillations are due to the pressure waves (rarefaction and compression waves) which propagate back and forth in the tank interacting with the tank structure.

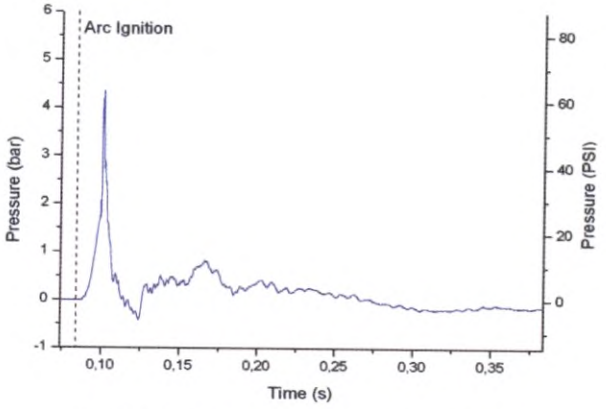

Test 23: Experiment – Pressure close to the arc

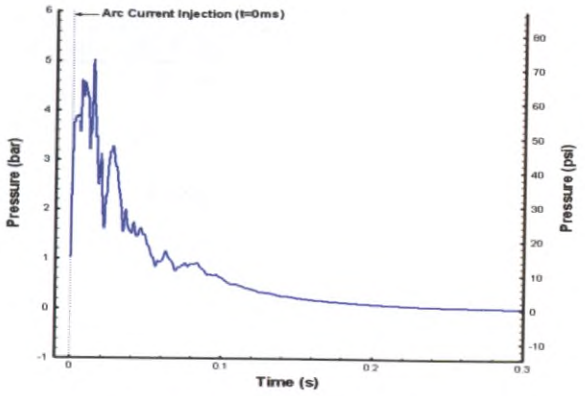

Test 23: Simulation – Pressure close to the arc

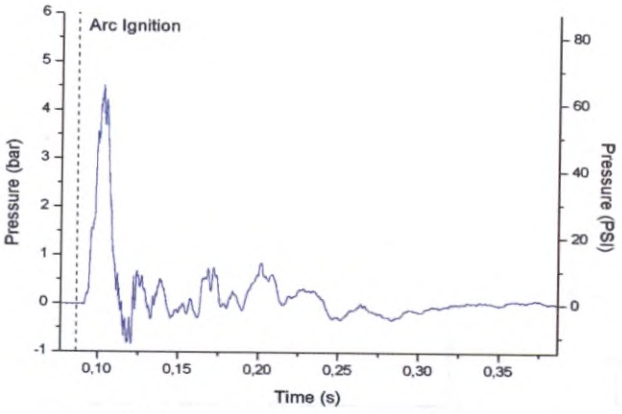

Test 31: Experiment – Pressure close to the arc

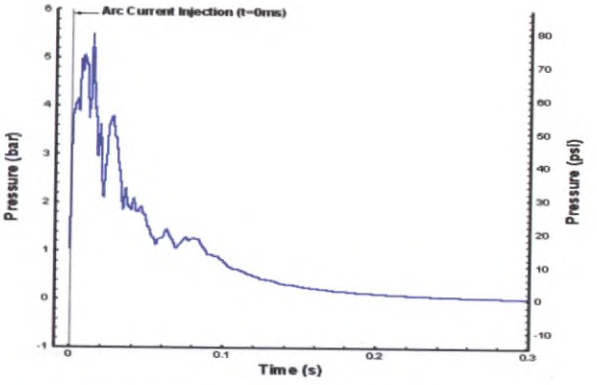

Test 31: Simulation – Pressure close to the arc

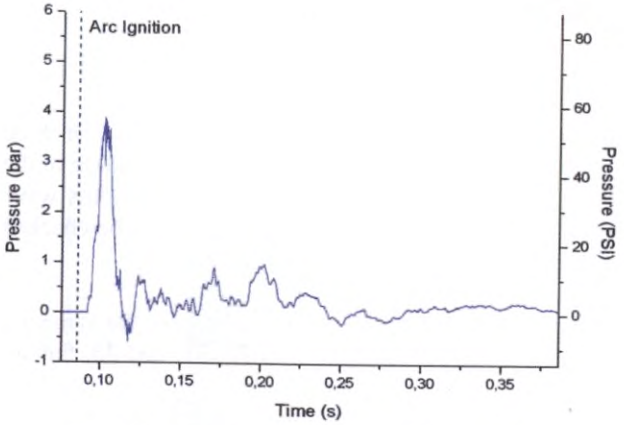

Test 33: Experiment – Pressure close to the arc

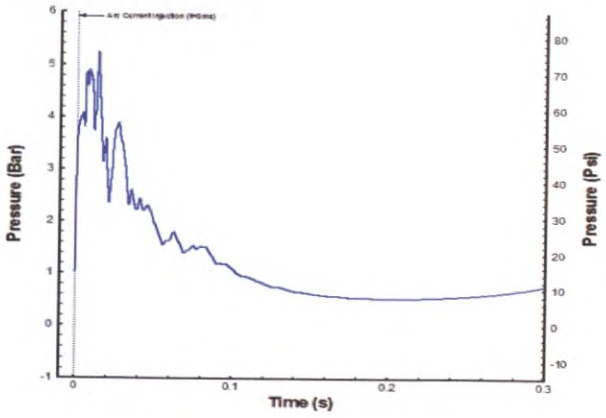

Test 33: Simulation – Pressure close to the arc

Figure 18 : Geometry influence on pressure profiles

If the transformer had not been equipped with the TP, the inner average pressure would have risen to the static overpressure withstand limit, and the transformer would have exploded. The pressure profiles displayed in Figure 19 show that, after the arc feeding, the average pressure remains close to an equilibrium state equal to *7 bar (100 psi)*. The static withstand limit pressure is thus reached, and the tank ruptures as soon as the tank wall elasticity limits are over, i.e. as soon as the tank walls cannot store any more mechanical energy due to the pressure increase.

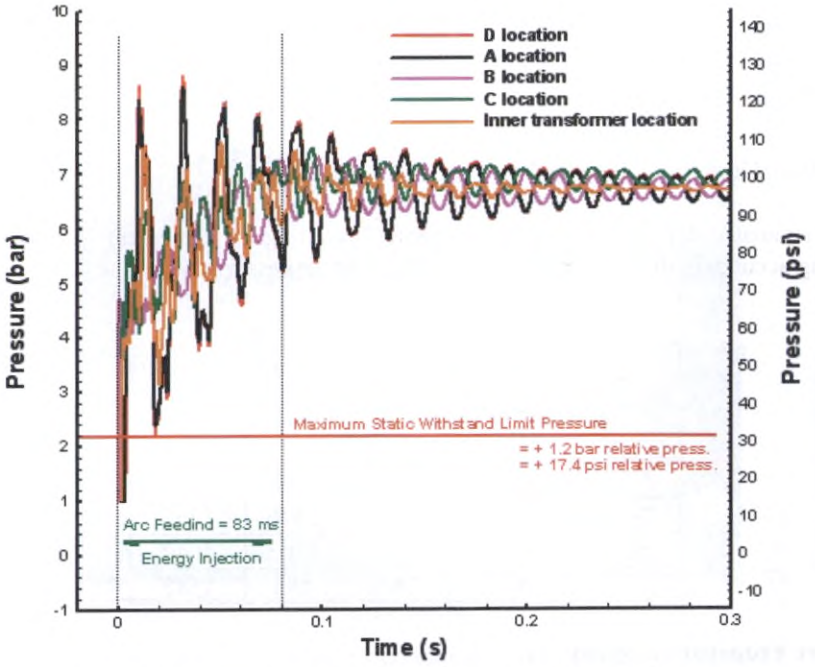

Figure 19 : Pressure when the Tank is NOT Equipped with the TP

All these similarities show that the numerical tool is reliable to describe the pressure evolution during a low impedance fault in a transformer as well as to describe the TP influence and operation on the inner pressure that prevents the transformer explosion. The numerical approach validation is completed by the following quantitative study.

4.4.5. Experiment/Simulation Quantitative Comparison

This comparison relies on the study of several TP operation criteria. The following study thus focuses on maximum pressure peaks, pressure gradients and depressurisation time.

- **Pressure**

The experimental as well as the simulated pressure peaks and gradients are summed up in Table 6. The relative error shows that the simulations and the experiments are in very good agreement. The numerical environment is thus reliable concerning the maximum pressure reached inside the transformers during a low impedance fault.

The simulation parameters are always chosen in order to study the TP operation and its efficiency for the most severe conditions. In Table 6 the numerical and experimental pressure gradients are stated. The simulated gradients are slightly overestimated when considering tests 23, 24, 31, and 33, but are in the range of the experimental gradients recorded during the CEPEL tests (from *100 bar/s* i.e.*14500 psi/s* to *4400 bar/s* i.e. *63800 psi/s*). The transformer tank was thus numerically subjected to more violent phenomena than during the experiments. The simulations show that even in these very severe conditions, the TP is able to depressurise the tank and prevent the transformer explosion.

Table 6 : Pressure Peaks and Pressure Gradients

Tests	Relative Error	Absolute Pressure Peak close to the Arc (simulation)		Absolute Pressure Peak close to the Arc (experiment)		Pressure Gradients (simulation)		Pressure Gradients (experiment)		Ratio Sim./Exp.
		bar	*psi*	*bar*	*psi*	*bar/s*	*psi/s*	*bar/s*	*psi/s*	
23	**6 %**	5.03	73	5.31	77	1300	18850	442	6410	2.9
24	**15 %**	3.45	50	3	43.5	1100	15950	97	1406	11.3
31	**1.2 %**	5.5	80	5.45	79	2120	30740	847	12281	2.5
33	**7.4 %**	5.24	76	4.88	70.76	2080	30160	392	5684	5 .3

- **Depressurisation Time**

Experimental and simulated depressurisation times (Table 7) are in good agreement. The numerical tool is thus reliable in depicting accurately the TP operation, influence, and depressurisation.

Table 7 : Depressurisation Time

Tests	Depressurisation Time		Experimental Wave Speed	
	(simulation)	(tests)		
	Ms	*ms*	*m/s*	*ft/s*
23	57.4	36.9	686	1267
24	37.5	19.7	2576	8452
31	59	73.4	1203	3949
33	78	76.9	483	1585

- **Pressure Wave Propagation Speed**

This parameter governs the wave dynamics because the wave velocity is very close to the speed of sound. In the modelling, the speed of sound remains equal to *1200 m/s* (*3937 ft/s*), which is physically true for oil without impurities. Nevertheless, during the experiments the waves' speeds changed in huge proportions because of oil pollution as stated in Table 7, and explained in section 4.3.3: For the considered tests (23, 24, 31, and 33) the theory from [25] is still in accordance with the experimental values which range from *483 m/s* to *2576 m/s* (*1584 ft/s* to *8451 ft/s*).

The differences between experiments and simulations regarding the waves' speeds (cf. Figure 15), the pressure gradients and the depressurisation times are thus the result of the pollution in the experimental oil during the tests.

- **Conclusion Regarding the Experiment/Simulation Quantitative Comparison**

The comparison between numerical and experimental results shows that the numerical and mathematical environments are reliable to describe the TP operation and the tank depressurisation by the TP. It shows the TP efficacy to prevent the tank explosion. The model can thus be used to illustrate the TP operation on very large transformers.

5. Transformer Explosion Prevention for Extrapolated Arcing and Operating Conditions

In this section, an illustrative example of fault on a large transformer (750MVA) is presented.

5.1. Geometry and Numerical Parameters

The 750 MVA transformer dimensions are displayed in Figure 20. The mesh is thus composed of 18 rectangular and trapezoidal blocks. The studied configuration corresponds to the worst case where the electrical arcing is ignited in location C. In other words, the arc and the gas bubble appear in the lower part of the transformer, far from the TP (Figure 20).

The maximum distance between the TP and the arc ignition is the key-parameter. In the case of the CEPEL tests, for T3 transformer, the biggest of the three, this distance was *8.5 m (28 ft)*. In the case of this 750 MVA transformer geometry, this distance is about *15 m (49 ft)*, twice the distance considered in the case of T3 transformer. In conclusion, the extrapolation is only of an order of 2, instead of an order of 37. The RD calibrated static pressure is set at *+1.2 bar* (*17.4 psi*).

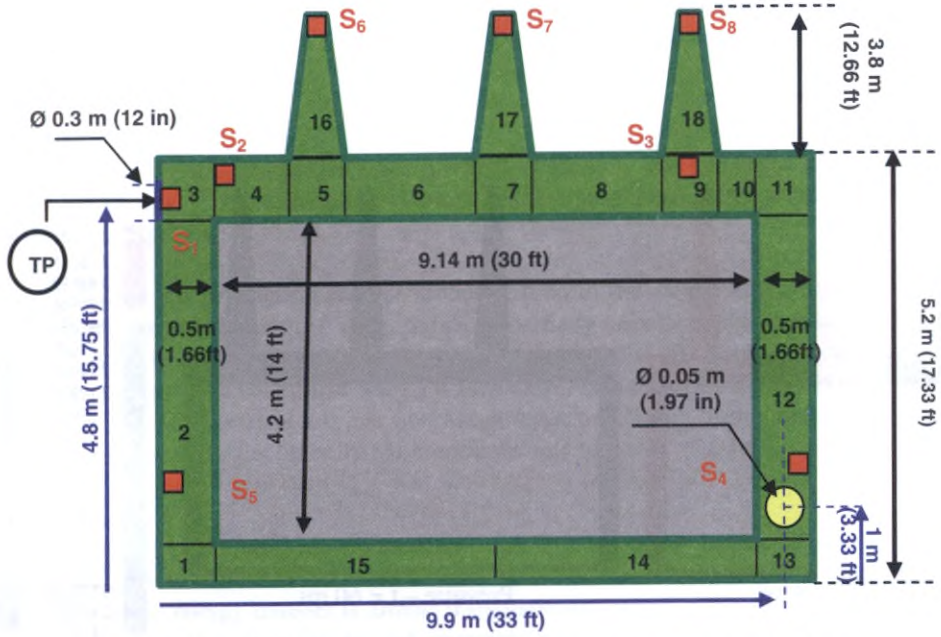

Figure 20 : Initial and boundary conditions, pressure sensors locations

Eight pressure sensors are placed into the tank to evaluate the pressure behaviour at several locations (Figure 20).

5.2. Results

A 70 kA arc is applied to the system for 70 ms, which is illustrative of harsh fault conditions. The pressure profiles are displayed in Figure 21 and Figure 22. The maximum pressure reached during this simulation is higher than *5.5 bar* (*80 psi*) in one of the bushings and *4.2 bar* (*61 psi*) close to the arc. The major value in the bushing is due to its geometry (wave-guide). The time for the wave to be propagated from the arc to the TP is *13.86 ms*.

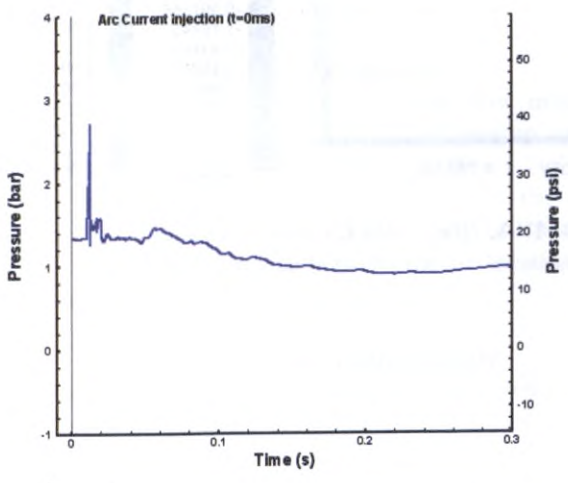

Figure 21 : 750MVA – Pressure close to the TP

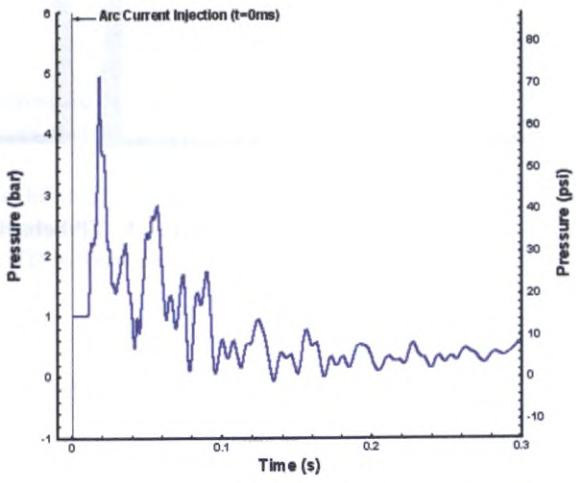

Figure 22 : 750 MVA – Pressure in location S6

The depressurisation time is *60 ms*, which is very acceptable for such a tank size. The pressure repartition informs us about the way the wave concentrated in any locations into the tank. The Figure 23 shows the interaction of the pressure wave with the TP after *14 ms*. After *60 ms*, the TP almost decreases the pressure under the *0.7bar* (*10.15 psi*) level in the entire tank, even if the electrical arcing is still supplied (pressure rise close to the bubble location). Even with a higher current (*70kA* instead of *15kA* for CEPEL tests) applied for *70 ms*, the TP succeeds in depressurizing the tank in few milliseconds since the pressure remains under the average withstand limit of the structure.

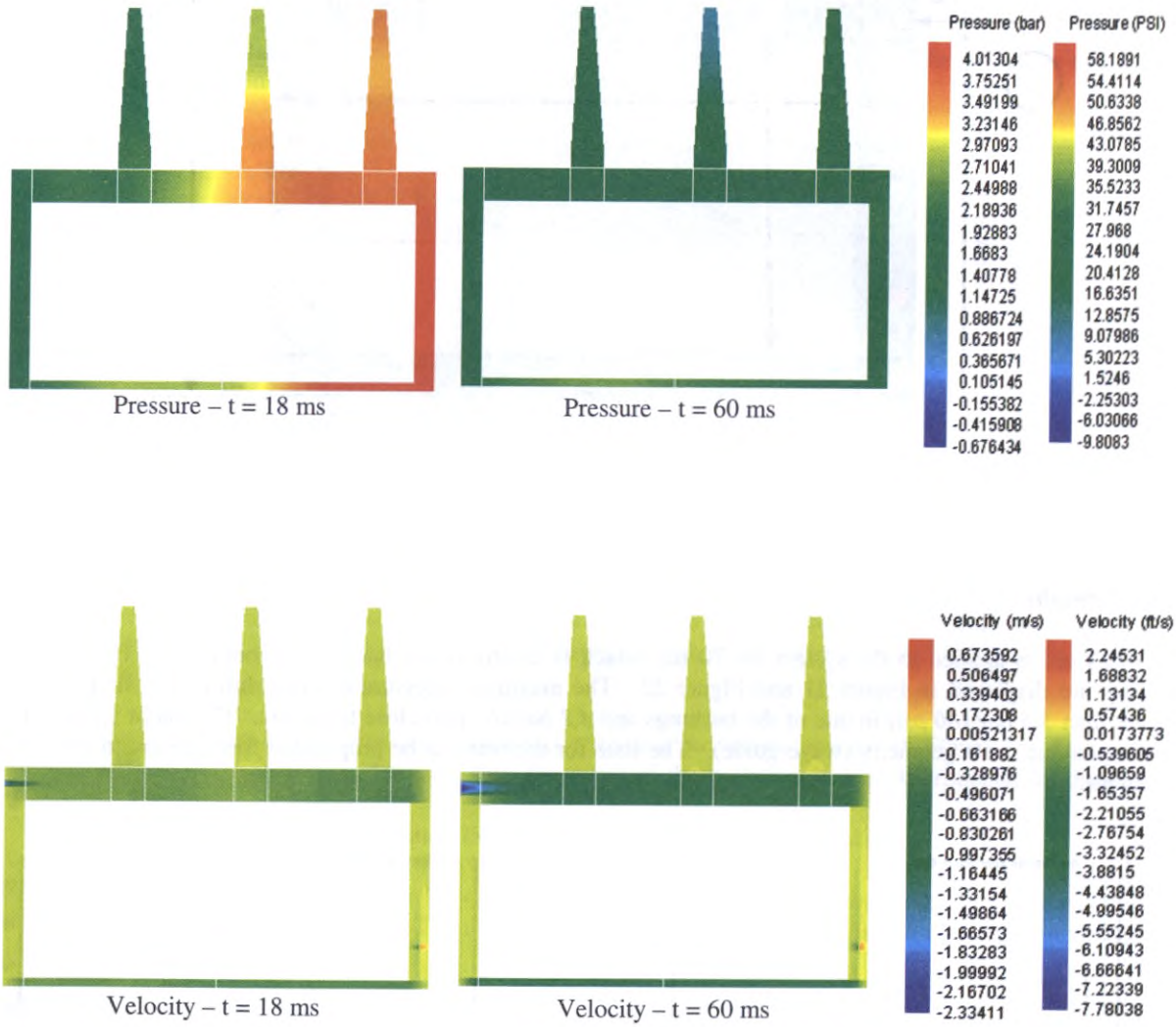

Figure 23 : TP behavior – 750 MVA, *70 ms*, *70 kA*, *C*

6. Conclusion

An essential step for SERGI is to show the TRANSFORMER PROTECTOR efficacy for all transformers and all types of rupture of insulation. Its research program philosophy is thus to maintain a strong connection between experiments and the theoretical developments.
The MTH model was upgraded in order to describe compressible two-phase flows, the pressure wave propagation inside liquids and gases, and to simulate the TP depressurisation process.

To verify calculations and simulations, CEPEL performed 34 experimental tests under low impedance faults. For each parameter, the following test results were found:

6.1. The Gas Generation

The gas volume generated during an electrical arc has been evaluated. The generated gas volume is a logarithmic function of the arc energy. This correlation is more reliable than linear extrapolations published up to day because it is based on experiments.

It is also shown that the gas production is huge at the creation of the electrical arc because of the intense heat exchange between the arc and the liquid. Then, the arc is partially or completely surrounded by gas. As a result, the arc energy is used to heat up the gas (thermal agitation), to crack the oil vapour into smaller molecules, and to change the gas into a plasma. Less and less energy is thus transferred to the dielectric oil for it to evaporate.
Consequently, for a *100 MJ* electrical arc, the first Mega Joule transferred to the dielectric oil generates *2.3 m^3 (81.2 ft^3)* of explosive gas, while the other 99 MJ contribute only to *2.0 m^3 (71.1 ft^3)*.

6.2. Pressure Peaks

Only one main pressure peak has been noticed for each test. Indeed, as the first vaporisation is a non-equilibrium phenomenon, it is more violent than the almost-at-equilibrium vaporisation occurring once the arc is ignited. Indeed, the initial energy transfer is almost instantaneous, and so is the phase change. The created gas has no time to expand and reach the pressure and temperature equilibrium with the surrounding oil. Because of the oil inertia, the gas is very quickly pressurised, which generates the first very strong pressure waves.
As it is more difficult to vaporise a liquid than to crack oil vapour, the arc location would mainly remain in the gaseous phase after its ignition. The vaporisation which happens after the gas bubble appearance is smoother and do not really generate physical conditions such as the ones in the very first arc instants. The secondary pressure variations are thus the result of the overlapping waves and structure influence combined with the smooth gas generation influence on pressure.
When comparing tests for which pressure peaks respectively equal *+8 bar (+116 psi)* and *+8.8 bar (127 psi)*, the corresponding arc energies vary within on order 10 of magnitude (*0.1 MJ* and *1 MJ* respectively).

6.3. Correlation between Arc Energy and Dynamic Pressure

The two above arguments demonstrate that the arc energy is not the key parameter to avoid transformer tank explosion as the gas production is huge only during the first Mega Joule, the pressure peaks amplitude does not increase significantly versus the arc energy.

6.4. The Pressure Wave Propagation

As predicted by the physical two-phase flow model, the pressure is not homogeneous in the transformer. Moreover, the study of the experimental pressure curves shows that the tank structure has an influence. This influence is noted as well with the simulations.

- The displacement of the shock wave in the tank is exhibited, demonstrating that the pressure waves propagate at finite speed experimentally, in agreement with theory.
- The maximum distance between the arc location and the TP is thus the parameter that matters the most for the TP to activate.

6.5. Tank Resistance to Dynamic Pressure

The following unknown key parameters have been discovered during the CEPEL tests:

- The tank resistance to dynamic pressure amplitude, the walls and components elasticity such as bolts or welding has been tested for pressure peaks up to 10 times over the static pressure limit.
- The tank resistance to dynamic pressure peaks duration was tested for 4 times longer than for the biggest existing transformer.

To achieve this results air was added to oil, as 1% of air inside the dielectric oil reduces the shock wave speed by a factor of 10, from *1200m/s (4000ft/s)* to *128m/s (426ft/s)*. During the tests, 0.5% ± 0.5% of air was added.

During the CEPEL tests, the highest activation time is 57 milliseconds for a travelling distance of 4 meters *(m)*. With normal, non-polluted transformer oil, the activation time would be approximately 6 milliseconds. In the case of the tests, the tank has withstood the dynamic pressure 10 times longer than with non-polluted oil. As an illustration, with normal transformer oil, 57 milliseconds correspond to a shock wave maximum distance to travel of *68 m (220 ft)*. Obviously, such transformer does not exist as it would be 4.5 times bigger that the *750 MVA* transformer used for simulations in section 5.

- The 3 transformer used by CEPEL have withstood 10 tests each in the worst conditions and, as stated by the CEPEL Test Certificate :*"Therefore, We state that for all the tests, the TRANSFORMER PROTECTOR, successfully prevented the transformer explosion, and prevented any kind of damage or permanent tank deformation."*

6.6. The TP Efficacy

The ability of the TRANSFORMER PROTECTOR to avoid tank explosion during low impedance faults has been demonstrated:

- The higher the pressure gradients are, the faster the TP operates.
- The very low inertia of the TP to open in less than 2 milliseconds for all pressure gradients has been demonstrated. While the whole tank can withstand pressure waves during at least 57 millisecond, the TP operates as soon as the pressure peak meet the Rupture Disk.
- When the TP operates the pressure peak is down to the static pressure calibration level in approximately 3 milliseconds. This confirms the calculated value of 3.5 milliseconds *(ms)* obtained with the MTH Model and published by SERGI in 2001 [18].
- On average, the TP depressurises the tank in *116 ms*, with a minimum of *19 ms* and a maximum of *347 ms*.
- As soon as the TP has activated, the arc can still be fed for a very long time, and the pressure remains at harmless levels for the transformer tanks. This was already emphasized by SERGI in 2001 [18] where it was demonstrated that for a *236 kA* short-circuit, an opening of *0.15 m (8 in)* was sufficient to evacuate the energy during a steady feeding of the electrical arc by the inertia of the generator.

6.7. The MTH Model Dynamic Pressure and Shock Wave Propagation

There are so many different tank geometries and transformer characteristics that it is impossible to test experimentally every transformer fault configuration. The numerical tool easily simulates several geometries, physical and electrical conditions for a transformer subjected to a low impedance fault. The model is validated with experimental tests chosen for their severe conditions for the TP. This validation relies on the study of several TP operation criteria:

- Pressure peaks: The error between experimental and simulated pressure peaks is low;
- Pressure gradients: The simulated gradients are in the range of the ones recorded during the CEPEL tests;
- Depressurisation times: The simulated depressurisation times are in very good agreement with the experimental results.

The numerical tool is thus reliable in depicting accurately the TP operation, influence, and depressurisation.

Once validated, the numerical tool enabled SERGI to simulate pressure rise due to electrical faults inside a transformer in various situations. A *750 MVA* transformer was chosen to simulate the TP behaviour in extrapolated operating conditions. The maximum distance between the worst electrical arc location and the TP during the CEPEL tests was *8.5 m (28 ft)* and for the simulation into a *750 MVA* transformer, *15 m (49 ft)*.

For the *750 MVA* transformer, a *70kA* short-circuit was considered during *70ms*. The pressure peak was equal to *5.5 bar (80 psi)*, the TP had activated after *14 ms*, and the transformer tank was depressurised in *60 ms* by the TP.

The simulation tool helps to understand transformer explosions, to design and improve the TRANSFORMER PROTECTOR.

7. References

[1]. R. ABGRALL, "*How to prevent pressure oscillations in multi-component flow calculations: A quasi conservative approach*", Journal of Computational Physics, vol. 125, pp. 150-160, 1996.

[2]. G. ALLAIRE, S. CLERC & S. KOKH, "A *Five Equation Model for the Simulation of Interfaces between Compressible Fluids*, Journal of Computational Physics, vol. 181, 2, pp. 577-616, 2002.

[3]. M.R. BAER & J.W. NUNZIATO, "*A Two-phase Mixture Theory for the Deflagration to Detonation Transition in Reactive Granular Materials*", International Journal of Multiphase Flow, vol. 12, 6, pp. 861-889, 1986.

[4]. N.P. CUK, "*Oil Tank Explosion Resistance*", CEA No. 149D491, Powertech Labs Inc., Surrey, B.C., June 1990.

[5]. F. DUBOIS, "*Boundary conditions and the Osher scheme for the Euler equations of gas dynamics*", internal report CMAP 170, Ecole Polytechnique, Palaiseau, France, 1987.

[6]. E. GODLEWSKI & PA. RAVIART, "*Numerical Approximation of Hyperbolic Systems of Conservation Laws*", Press, Applied Mathematical Sciences, vol. 118, ed. Springer Verlag, Berlin, 1996.

[7]. S.K. GODUNOV, "*A Finite Difference Method for Numerical Computation of Discontinuous Solutions of the Equations of Fluid Dynamics*", Math Sb., vol. 47, pp. 357-393, 1959.

[8]. O.R. HANSEN, "*SEBK Project: Results from Phase 2 Laboratory Scale Experiments*", Gexcon, May 2001.

[9]. A.K. KAPILA, R. MENIKOFF & D.S. STEWART, "*Two-phase Modelling of Deflagration to Detonation Transition in Granular Materials: Reduced Equations*", Physics of Fluids, vol. 113, 10, pp. 3002-3024, 2001.

[10]. O. LE METAYER, "*Modélisation et résolution de la propagation de fronts perméables – Application aux fronts d'évaporation et de detonation*", Ph. D. Thesis, Université de Provence, Mechanics & Energy, Marseille, France, 2003.

[11]. J. MASSONI, R. SAUREL, B. NKONGA & R. ABGRALL, "*Proposition de méthodes et de modèles eulériens pour les problèmes à interfaces entre fluides compressibles en présence de transfert de chaleur*"/ "*Eulerian model and method proposal for flows with interfaces in presence of heat transfers*", International Journal Of Heat and Mass Transfers, vol. 45, 6, pp. 1287-1302, 2002.

[12]. A. MURRONE & H. GUILLARD, "*A Five Equation Reduced Model for Compressible Two-phase Flow Problems*", Journal of Computational Physics, vol. 202, Issue 2, 2005.

[13]. R. SAUREL & R. ABGRALL, "*A multi-phase Godunov Method for Compressible Multi-fluid and Multi-phase flows*", Journal Of Computational Physics, vol. 150, pp. 425-467, 1999

[14]. R. SAUREL & R. ABGRALL, "*A Simple Method for Compressible Multi-fluid Flows*", SIAM J. of Scien. Comput., vol. 21, 3, pp. 1115-1145, 1999.

[15]. R. SAUREL & O. LEMETAYER, "*A Multi-phase Model for Compressible Flows with Interfaces, shocks, detonation waves and cavitation*", Journal Of Fluid Mechanics, vol. 431, pp. 239-271, 2000

[16]. SERGI, "*Development of a Magneto-Thermo Hydrodynamic Model and Design of a Transformer, On load Tap Changer and Bushing Oil Cable Box, Explosion and Fire Prevention*", IEEE Publication, ref. rpiip01a, 1999.

[17]. SERGI, "*Comparison of the SERGI developed Magneto-Thermo Hydrodynamic Model results with measurements made on a 160KVA Transformer*", IEEE Publication, ref. rpijp01a, 2000.

[18]. SERGI, "*Study and Design of Power Plant Transformers Explosion and Fire Prevention*", Australia, TechCon 2001, ref. rpitp05a, 2001.

[19]. SERGI, "*Transformer Relief Valves efficiency calculations by comparison to the SERGI TRANSFORMER PROTECTOR during short-circuits*", ref. rpisp01a.

[20]. SERGI, "*Transformer Explosion and Fire, Guideline for Damage Cost Evaluation, TRANSFORMER PROTECTOR Financial Benefit*", ref. fTPoa03a, 2004.

[21]. SERGI, "*Study of the Pressure Wave Propagation and Depressurisation Process for an Electrical Transformer Subjected to Internal Arcing, Design of a Decision-Making Management Tool for Transformer Explosion Prevention*", ref. Arpiyp02a, 2006

[22]. SERGI, "*Pressure Wave Propagation in a Transformer Tank: Numerical Simulations, Experiments, and Extrapolations*", ref. Fre30rr09a, 2005.

[23]. N. THEVAND, "*Contribution à l'Etude Numérique des Ecoulements Instationnaires et Visqueux de Mélanges Gaz-Particules Dilués*", Ph. D. Thesis, Université de Provence, Méchanics & Energy, Marseille, France, 1999.

[24]. E. TORO, "*Riemann Solvers and Numerical Methods for Fluid Dynamics*", Press, ed. Springer Verlag, Berlin, 1997.

[25]. G. WALLIS, "*One Dimensional Two-Phase Flow*", Press, ed. Graw Gill Company, New York, 1969.

8. Biography

Dr. Guillaume PERIGAUD
Research Department Manager, SERGI-Holding
Diploma of Mechanical Engineering, and MSc in Transfers and Fluid Mechanics, ECN, Nantes, France (2000).
Doctor in Mechanics and Energetics, Université de Marseille I, France (2003).

Eng. Héloïse CUNY
Research Engineer, SERGI-Holding
Diploma of Mechanical Engineering, and MSc in Dynamics and Complex Fluids, ENSAM, Paris, France (2004).

Eng. Sylvain Prigent
Development Department Manager, SERGI-Holding.
Saint-Louis Polytechnic Institute, EPMI, Paris, France (1999).

Dr. Philippe MAGNIER
SERGI-Holding Chairman
M.B.A., CPA, Paris (1988).
Doctor in Nuclear Physics, Université Paris Orsay (1974).